Paleoceanography and Paleoclimatology

RESEARCH ARTICLE
10.1029/2022PA004605

Impact of Deep Water Formation on Antarctic Circumpolar Transport During Gateway Opening

D. R. Munday[1], **I. Sauermilch**[2], **A. Klocker**[3], **and J. M. Whittaker**[4]

[1]British Antarctic Survey, Cambridge, UK, [2]Department of Earth Sciences, University of Utrecht, Utrecht, The Netherlands, [3]NORCE Norwegian Research Centre, Bjerknes Centre for Climate Research, Bergen, Norway, [4]Institute for Marine and Antarctic Studies, University of Tasmania, Hobart, TAS, Australia

Key Points:

- Deep water formation in the Southern Ocean enhances Antarctic Circumpolar Current transport
- Circumpolar transport is possible even with large obstacles to the flow
- Deep water formation enables transport north of Australia with a narrow Tasman Gateway

Correspondence to:
D. R. Munday,
danday@bas.ac.uk

Citation:
Munday, D. R., Sauermilch, I., Klocker, A., & Whittaker, J. M. (2024). Impact of deep water formation on Antarctic circumpolar transport during gateway opening. *Paleoceanography and Paleoclimatology*, *39*, e2022PA004605. https://doi.org/10.1029/2022PA004605

Received 20 DEC 2022
Accepted 12 MAY 2024

Author Contributions:
Conceptualization: D. R. Munday
Formal analysis: D. R. Munday
Software: D. R. Munday
Visualization: D. R. Munday, I. Sauermilch, A. Klocker
Writing – original draft: D. R. Munday, I. Sauermilch, A. Klocker, J. M. Whittaker
Writing – review & editing: D. R. Munday, I. Sauermilch, A. Klocker, J. M. Whittaker

Abstract Ambiguity over the Eocene opening times of the Tasman Gateway and Drake Passage makes it difficult to determine the initiation time of the Antarctic Circumpolar Current. If the Tasman Gateway opened later than Drake Passage, then Australia may have prevented the proto-ACC from forming. Recent modeling results have shown that only a relatively weak circumpolar transport results under Eocene surface forcing. This leads to warm and buoyant coastal water around Antarctica, which may impede the formation of deep waters and convective processes. This suggests that a change in deep water formation might be required to increase the density contrast across the Southern Ocean and increase circumpolar transport. Here we use a simple reduced gravity model with two basins, to represent the Atlantic and the Pacific. This fixes the density difference between surface and deep water and allows us to isolate the impact of deep water formation on circumpolar transport. With no obstacle on the southern boundary the circumpolar current increases its transport from 82.3 to 270.0 Sv with deep water formation. Placing an Antipodean landmass on the southern boundary reduces this transport as the landmass increases in size. However, circumpolar flow north of this landmass remains a possibility even without deep water formation. Weak circumpolar transport continues until the basin is completely blocked by the Antipodes. When the Antipodes is instead allowed to split from the southern boundary, circumpolar transport recovers to its unobstructed value. Flow rapidly switches to south of the Antipodes when the gateway is narrow.

1. Introduction

In the modern world, the Southern Ocean is the only body of water to completely circumnavigate the globe. In doing so it connects the other ocean basins via its major current systems, the Antarctic Circumpolar Current (ACC, in the horizontal plane) and the Residual Meridional Overturning Circulation (RMOC, in the vertical-meridional plane). The volume transport of the ACC, at around 137 ± 7 Sv (Sverdrup, 1 Sv = 10^6 m^3s^{-1} Meredith et al., 2011) or 173 ± 10.17 Sv including the near bottom flow measured by current meters (Donohue et al., 2016), is the largest observed for any modern current system. However, over geological time there has been major tectonic reorganization of Southern Ocean gateways, that is, the Tasman Gateway and Drake Passage. Changes to these gateways, in terms of their width and depth, could have a major influence on the strength of the ACC, or even preclude its existence (e.g., Baatsen et al., 2018; Hill et al., 2013; Kennett, 1977).

Unfortunately, there is considerable ambiguity to the opening time and evolution of both Southern Ocean gateways. For example, the opening of Drake Passage may span from 50 to 17 Ma (megaannum, 1 Ma = 10^6 years, Barker et al., 2007; Livermore et al., 2005), with a similar range for the inception of the ACC (Scher & Martin, 2006; Wei & Wise, 1992). Other measurements suggest that Drake Passage may have been open during the Cretaceous and subsequently closed prior to a later reopening (van de Lagemaat et al., 2021). Similarly, the earliest dates for a shallow opening of the Tasman Gateway are also 50 Ma (Bijl et al., 2013) with a deep seaway between the Indian and Pacific basins in place by 35–32 Ma (Royer & Rollet, 1997) and the potential for a relatively rapid subsidence history (Stickley et al., 2004). Dredged sediment samples further suggest that rapid ACC flow through the Tasman Gateway might not have occurred for another 3–5 million years, when the gateway was aligned with the westerly wind jet (Scher et al., 2015). A hypothesis that was tested by shifting the zonal winds southwards in a model by Xing et al. (2022). This showed that aligning the winds with both Tasman Gateway and Drake Passage does increase circumpolar transport. On the north side of Australia, the Indonesian throughflow was likely open during the Eocene, narrowing after 30 Ma (Gaina & Müller, 2007). This may have worked as a "northern gateway" for a young ACC assuming an open Drake Passage >30 Ma (Sijp et al., 2011).

This evidence suggests that the inception and early evolution of the ACC's transport was likely affected by a series of tectonic changes, over millions of years, to the sea-floor bathymetry and ocean gateways.

There are strong theoretical grounds to expect the position of the ACC to be tied to major bathymetric obstacles (Marshall, 1995). However, simple models and theory also show it has the ability to migrate up to several thousand kilometers to follow wind forcing (Allison et al., 2010; Marshall et al., 2016). This led Munday et al. (2015) to suggest that the opening of the Tasman Gateway might not be a prerequisite for a circumpolar current, as has sometimes been assumed in the literature (see, e.g., Barker et al., 2007; Sijp et al., 2014). The idealized channel model of Munday et al. (2015) indicates that overlapping continental barriers do not prevent circumpolar transport in the range of several 10's of Sv, as long as there is a traceable circumpolar path around the continents. Using plausible bathymetric reconstructions, and forcing derived from the coupled climate model of Hutchinson et al. (2018), Sauermilch et al. (2021) show that both gateways must be open and deeper than 300 m to allow significant circumpolar flow. In their supplementary case with Australia attached to Antarctica, no circumpolar flow results. They hypothesize that initiation and/or strengthening of deep water formation and the continuously decreasing atmospheric carbon dioxide concentrations around Antarctica may play a role in the strengthening of the ACC to present-day conditions and in setting its transport. Lefebvre et al. (2012) also argue for the importance of deep water formation in the initiation of the ACC with sea-ice production caused by a gradual reduction in atmospheric CO_2 resulting in the creation of saline and cold water masses. This then increases the meridional density gradient across the Southern Ocean with the thermal wind response strengthening the ACC transport.

The presence of deep water formation/overturning has been shown to affect the strength of circumpolar transport in idealized models of the Southern Ocean (Howard et al., 2015; Stewart & Hogg, 2017; Youngs et al., 2019). In these examples, the circumpolar transport, regardless of the presence of deep water formation, differs from the observed transport of the ACC and the increase in the presence of deep water formation is modest. In the channel model of Stewart and Hogg (2017) the circumpolar transport increases by ∼20% with the addition of Antarctic Bottom Water (AABW) formation, depending on the details of the channel's bathymetry (a bump vs. a ridge blocking all *f*/*h* contours, see Section 2.3 for a discussion of the effect of *f*/*h* contours on ocean circulation). In the case of a channel with a ridge, the circumpolar transport is low at only 34.1 Sv in the absence of AABW formation. Youngs et al. (2019) report similar circumpolar transport in the absence of southern deep water formation, ∼22 Sv, in their quasi-geostrophic channel with a ridge. The addition of AABW formation increases this by ∼14–27%, with stronger overturning leading to a larger increase. The increase in circumpolar transport in Howard et al. (2015) when water mass transformation is included is much larger, in an absolute sense, at ∼100 Sv. However, this builds upon a circumpolar transport of ∼300 Sv when only wind forcing is applied, which translates to an ∼33% increase. The model of Sauermilch et al. (2021) and Xing et al. (2022) uses realistic Eocene bathymetry and forcing. Even the largest transport reported by Xing et al. (2022), for a deep Tasman Gateway and doubled wind forcing with the peak aligned with Drake Passage, is only 44.8 Sv, which would have to increase by ∼300% to match the ∼180 Sv estimate of Donohue et al. (2016) for the modern ACC.

Global climate change during the Late Eocene, and across the Eocene-Oligocene transition (34 Ma), is accompanied by progressive global cooling, including that of the deep water (see, e.g., Westerhold et al., 2020). This is interlinked with the reorganization of ocean circulation, as well as changes in the sources and strength of deep water formation. Uncertainties remain about the rate and location of deep-water formation during and prior to the Eocene. However, modeling and geochemical studies (primarily isotopic composition analyses on sediment cores) agree on a bipolar deep water formation; deep water is formed in the North and South Pacific, as well as in the Southern Ocean's Atlantic sector (see, e.g., Hague et al., 2012; McKinley et al., 2019; Thomas, 2004; Thomas et al., 2014; Via & Thomas, 2006).

Some evidence exists that during and prior to the Eocene, meridional overturning circulation (MOC) was active in the Pacific Ocean (albeit weaker than in the modern-day). This gradually switched to the Atlantic around 36 Ma and onwards (McKinley et al., 2019), potentially due to the opening of Arctic-Atlantic connections (Hutchinson et al., 2019). Locally focused bottom water formation took place offshore of Antarctica (Huck et al., 2017) and, with the onset of Antarctic-wide glaciation around 34 Ma, sea ice became present and Antarctic coastal waters cooled down. Together with the increased Antarctic-ward salt flux within the Ekman layer, the dense and cool water masses subsided to the abyssal plain regions offshore of Antarctic shorelines (Goldner et al., 2014). This

deep water formation enhanced the MOC and contributed to the global deep water cooling observed by oxygen isotope records (see, e.g., Westerhold et al., 2020).

The development of the proto-ACC has been linked to North Atlantic Deep Water (NADW) formation onset, affecting the MOC, as well as leading to deep-ocean circulation, and the onset of modern-like bipolar deep water formation (see, e.g., Via & Thomas, 2006). Small changes in Arctic-Atlantic gateway depths, such as the Greenland-Scotland Ridge, have also been linked to the initiation of NADW formation (Straume et al., 2022; Vahlenkamp et al., 2018). The closure of the Arctic may then lead to reorganization of the MOC and shift of deep water formation from the North Pacific to the North Atlantic (Hutchinson et al., 2019). A change in North Atlantic stratification, indicating increased convection, has even been dated to before Antarctic glaciation (Coxall et al., 2018). Oxygen isotope records suggest that from the early Oligocene onwards, ocean waters started to develop modern-day-like surface, intermediate, deep and bottom water layers, caused by the strengthening of the proto-ACC (Katz et al., 2011). The ACC initiation also leads to thermal differentiation between North Atlantic and Southern Ocean deep waters (Borrelli et al., 2014). As noted above, Lefebvre et al. (2012) argue for a role for deep water formation in ACC initiation, with brine rejection from sea-ice formation aiding its subsequent intensification due to salinity-driven enhancement of the across-Southern Ocean density gradient. Similar results are obtained by Ladant et al. (2014) with cooling triggered by Antarctica glaciation and sea-ice changes driving deep water formation and density structure alteration. The opening of Drake Passage has also been shown to alter the location of Southern Ocean convection and cause different patterns of heating/cooling in the ocean's basins as a result (Toumoulin et al., 2020). This suggests that there is indeed a strong link between ACC transport, deep water formation and the MOC, as hypothesized by Sauermilch et al. (2021), although here we restrict our attention to the influence of southern hemisphere deep water formation on the ACC.

The questions we seek to answer here are

1. Can the initiation of Southern Ocean deep water formation increase the circumpolar transport of the ACC to modern levels?
2. Can the presence of deep water formation lead to circumpolar transport when the Tasman Gateway is closed?

Given the uncertainty regarding continental geometry and surface forcing, we choose to investigate the above questions using an idealized numerical model in a process study framework. Our aim is not to simulate a circumpolar current in a realistically complex geometry, but to investigate the relevance of theoretical ideas based on the modern ACC to its inception and early history. By using a reduced gravity model with restoring to a shallow layer thickness near the southern continental boundary, we can choose the presence or absence of deep water formation without altering the density gradients present. This allows us to separate these two aspects of the argument of Lefebvre et al. (2012). This would not be possible in a more complex 3D model, since the combination of different forcing patterns would determine the presence/absence of deep water formation as an emergent property of the model solution. A reduced gravity model also has the benefit of allowing us to draw on a substantial body of literature regarding the spin-up and adjustment of the ACC (see, e.g., Allison, 2009; Allison et al., 2010, 2011), making for a well-understood framework to hang our problem on. The model is low resolution, and so parameterizes the mesoscale eddy field, which has implications for its representation of Southern Ocean circulation and dynamics (see Section 4 for a discussion on the role of mesoscale eddies). Its representation of basin geometry is necessarily, and deliberately, idealized and the reduced gravity formulation prevents the inclusion of bottom bathymetry impacts. This allows the consideration of a simpler, more tractable problem that can be interrogated with a large number of numerical experiments. This may pave the way for a more dynamically complex and bathymetrically rich investigation in the future.

In Section 2 we describe the details of our reduced gravity model and the diagnostic methods we apply to it. In Section 3, we discuss the results of the reduced gravity model experiments aimed at answering the above questions. We split these experiments into two sets. The first set, regarding the migration of the ACC around a landmass on the southern boundary as it increases in northwards extent (Sections 3.2), and the second set regarding a landmass separating from the southern boundary and migrating northwards (Section 3.3). We close with a summary of our conclusions and discussion of our results, plus the caveats that should be taken into account, in Section 4.

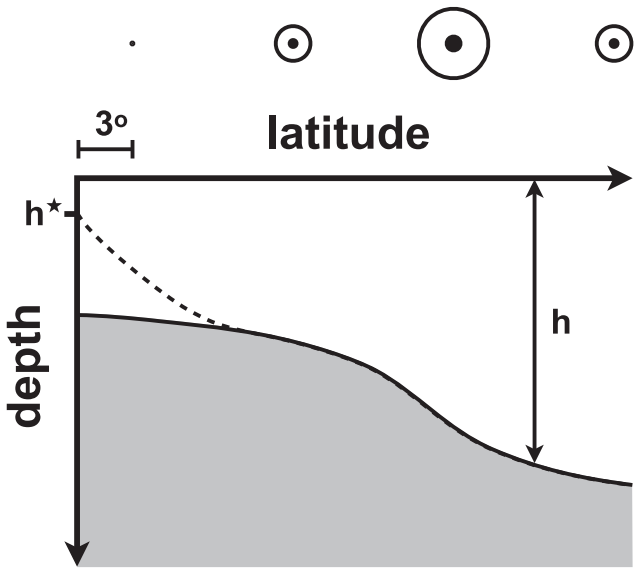

Figure 1. Schematic of a reduced gravity model with a single active layer of thickness h (in white) overlying a motionless abyss of infinite depth (gray). For the model used here, the wind is sketched as a series of circumpuncts and for some of our experiments layer thickness is restored toward $h^\star$ within 3° of the southern boundary, as indicated by the dashed line.

2. Methods

2.1. Model Numerics and Domain

For our idealized numerical experiments, we choose to use a reduced gravity model whose formulation is comprised of a single active layer overlying a motionless abyss of slightly denser water, as shown in the schematic of Figure 1. This abyss, shaded in gray in Figure 1, is assumed to be of infinite depth, such that its velocity can be considered to be zero, and to completely encompass any bathymetry. The thickness of the active layer, in white in Figure 1, is given by h, which can be interpreted as the effective pycnocline depth. Typically, it is simplest to consider the active layers as being warmer than the motionless abyss. This very simple representation of ocean stratification is the simplest that can support an ACC with a strong transport driven by thermal wind shear. It also serves as the under-pinnings of the heuristic model of Gnanadesikan (1999), which can be applied as a simple model of the MOC. Note that the model of Gnanadesikan (1999) is very simple and one process that it excludes is southern deep water formation, which is our focus here. Its treatment of the Southern Ocean in particular has been the subject of several papers that extend its original formulation (see, e.g., Cimatoribus et al., 2014; Johnson et al., 2007; Marshall & Zanna, 2014). Shakespeare and Hogg (2012) expand the model to have 3 layers, for a fuller description of a two cell overturning, and in doing so explicitly include southern deep water formation. The simple formulation and minimal nature of a reduced gravity model make it attractive on both theoretical and numerical grounds (Allison, 2009; Allison et al., 2010, 2011; Huber & Nof, 2006; Johnson et al., 2007; Jones & Cessi, 2016; Jones et al., 2011; Marshall et al., 2016; Nof, 2000a, 2000b, 2003; Nof & Van Gorder, 2003).

The momentum equation, Equation 1, and continuity equation, Equation 2, for our reduced gravity model are written in vector-invariant form and given by

$$\frac{\partial \mathbf{u}}{\partial t} + (f+\xi)\,\mathbf{k}\times\mathbf{u} = -\nabla B + \frac{1}{h}\nabla\cdot(A_H h\nabla\mathbf{u}) + \frac{\boldsymbol{\tau}}{\rho_0 h}, \tag{1}$$

$$\frac{\partial h}{\partial t} + \nabla\cdot(h\mathbf{u}) = \nabla\cdot(\kappa_{GM}\nabla h) + \frac{\kappa_v}{h} - \gamma\left(h - h^\star\right), \tag{2}$$

where $\mathbf{u} = (u, v)$ and h are the two-dimensional flow velocity and thickness of the active fluid layer, respectively. The Bernoulli potential, which is equivalent to pressure, is given by $B = g'h + \frac{1}{2}\mathbf{u}\cdot\mathbf{u}$, with $g' = g\Delta\rho/\rho_0$ being the reduced gravity. f is the Coriolis frequency and $\xi = \nabla\times\mathbf{u}$ is the vertical component of the relative vorticity. The Boussinesq reference density of the active layer is ρ_0 and the density difference between the active layer and the motionless abyss is $\Delta\rho$. The grid spacing is 1° in both longitude and latitude, so the zonal grid spacing in kilometers decreases toward the northern/southern high latitudes. The standard values used for the model parameters, along with details of the timestep, etc, are given in Table 1. Note that for reasons of numerical stability we found it necessary to halve the timestep for experiments without deep water formation.

The momentum equation, Equation 1, incorporates viscosity with a constant grid Reynolds number such that the viscosity, A_H, varies with latitude. This prevents the model from violating stability constraints near the northern/southern boundary where the longitudinal grid spacing is much smaller than the meridional grid spacing. Surface wind forcing of strength $\boldsymbol{\tau}$ is applied as a body force over the active fluid layer. The Coriolis and vortex force terms are calculated so as to conserve enstrophy and KE is calculated to also ensure its conservation.

The continuity equation, Equation 2, incorporates the Gent and McWilliams (1990) eddy parameterization (GM) as thickness diffusivity, written as an advective flux with a constant co-efficient of κ_{GM}. This acts as a zero-order eddy parameterization in this model framework and acts to reduce gradients in thickness in a similar manner to baroclinic instability, as it tends to flatten isopycnals. These simulations therefore have more in common with the 1° Supplementary cases of Sauermilch et al. (2021) than they do their 1/4° simulations, that is, they are viscous/

Table 1
Standard Parameter Values for Reduced Gravity Model

Parameter	Symbol	Value	Units
Diapycnal diffusivity	κ_v	10^{-5}	m^2/s
GM co-efficient	κ_{GM}	2,000	m^2/s
Grid length scale (mean grid spacing)	L	–	m
Grid Reynolds number	Re_Δ	0.0062	–
Grid spacing (long, lat)	$\Delta\lambda$, $\Delta\phi$	1,1	°
Horizontal viscosity	A_H	$\mathrm{Re}_\Delta L^2/4\Delta t$	m^2/s
Peak wind stress	τ_0	0.15	N/m^2
Reduced gravity	g'	0.02	m/s^2
Restoring thickness	$h^\star$	10	m
Restoring timescale ($1/\gamma$)	t_{restore}	10^6	s
Timestep	Δt	600/1,200	s

diffusive and lack resolved mesoscale eddies. The value chosen for κ_{GM}, 2,000 m^2s^{-1}, is as per Allison et al. (2010, 2011). It is within the range typically used in the ocean component of coupled climate models (see, e.g., Kuhlbrodt et al., 2007) albeit at the upper end of the range found by Visbeck et al. (1997). Note that Eden et al. (2007) find much larger values in subtropical gyres in an eddy-resolving model.

The model also includes a parameterization of diapycnal diffusivity as per Gnanadesikan (1999), with a constant co-efficient of κ_v. When the active fluid layer is thin, this acts to flux volume upwards and thicken the layer, which is equivalent to heat being fluxed downwards due to the active layer being warmer than the motionless abyss. The conversion of abyssal water to the warmer water that makes up the active layer to increase h requires heat to be transported downwards because when the abyssal water enters the pycnocline it must increase its temperature to match that of the active layer. We neglect any parameterization of northern sinking, as included in the model of Gnanadesikan (1999) or those of Nof (2000b, 2002, 2003), as per Allison (2009) and Allison et al. (2010, 2011). This is on the basis that the most likely scenario for the Eocene ocean lacks deep water formation in the North Atlantic (Zhang et al., 2022).

Within ~3° of the southern boundary, as shown in Figure 1 and by the dark gray line in Figure 2, the thickness of the active layer is strongly restored to a small value, given by $h^\star$ (see Table 1). This restoring takes place with a timescale of t_{restore} and leads to the thickness of the active layer becoming small in this region. This is intended to represent the outcropping of the pycnocline, as happens in the modern Southern Ocean, when intense cooling leads to deep water formation. In practise, this intense cooling would be likely to also change the density contrast across the Southern Ocean. In our reduced gravity framework, this would be equivalent to changing g' and this would also increase the circumpolar transport. If the main pycnocline was already outcropping at the surface, increasing the reduced gravity would be a more realistic way of simulating the onset of deep water formation. However, based on our previous work with a more complex model (Sauermilch et al., 2021; Xing et al., 2022, 2023), isopycnals tend to be very flat and shallow in the absence of deep water formation and restoring to a small value of h would be more reflective of the initiation of deep water formation in this scenario. For numerical reasons, the value of $h^\star$ is also enforced as a minimum layer thickness throughout the domain. This prevents

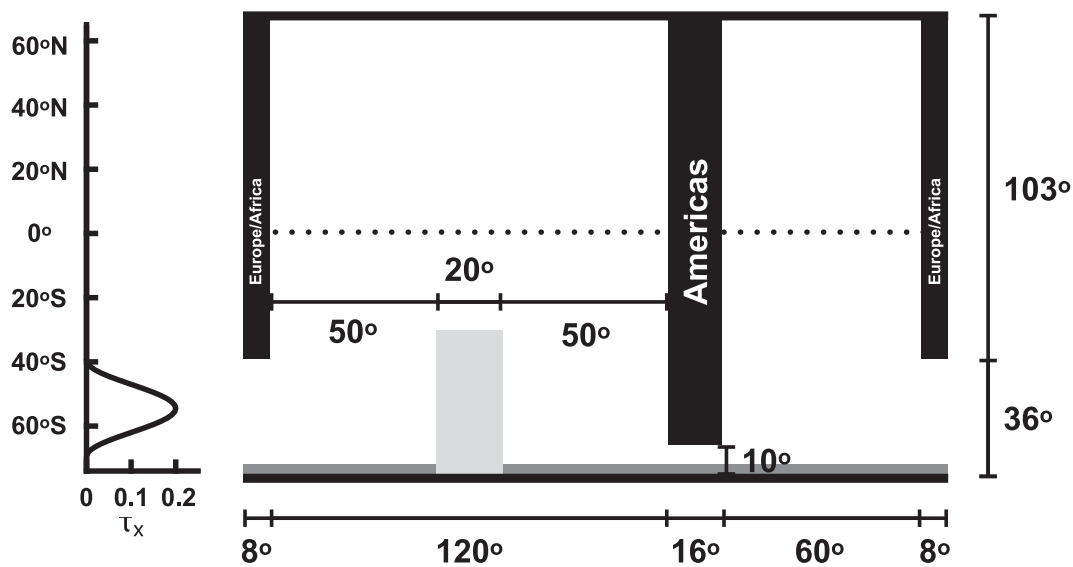

Figure 2. Schematic of the model domain and the applied wind stress. The solid northern/southern boundaries and the partial barriers described in the test are in black. The area shaded light gray is the "Antipodes" and the dotted line is the Equator. The dark gray line shows where the deep water formation is applied along the southern boundary. The line graph to the left is the applied zonal wind stress.

numerical instability if the layer outcrops (goes to zero thickness) and, roughly speaking, parameterizes buoyancy forcing and/or mode water formation. This term in Equation 2 represents deep water formation via buoyancy loss to the atmosphere near Antarctica. Reducing the thickness of the active layer in this way represents a loss of heat because water must be moving from the active layer to the abyss. This abyssal water is colder and denser, and so the reduction of h is analogous to the active layer losing heat. By setting $t_{\text{restore}} = \infty$ ($\gamma = 0.0$), we are able to disable deep water formation and test our hypotheses by transitioning between the two extreme cases of no deep water formation and strong circumpolar deep water formation.

The thickness restoring and diapycnal diffusion terms in the model drive an MOC with a sink of active layer thickness near the southern boundary being returned to the north by the diapycnal diffusion. The rate at which volume is removed/added is not constrained a priori and the model is allowed to adjust to its own equilibrium. An alternative approach would be to directly constrain the overturning, as per Youngs et al. (2019), by removing a set volume flux near the southern boundary and returning it to the north. This would then allow us to test how the changing MOC would impact the circumpolar transport. We have chosen the former for two main reasons: (a) depending upon details of the model configuration, removing volume near the southern boundary with a set flux could locally reduce the active layer thickness to zero, which would be numerically difficult, (b) it is unclear what MOC we should prescribe, since the Eocene overturning is thought to be different to that of the modern ocean and the details vary between different estimates (Zhang et al., 2022).

The model equations are stepped forwards in time using the Adams-Bashforth 3rd order scheme, due to its advantages over a centered-in-time scheme (Durran, 1991). The continuity equation is discretized using centered 2nd order differencing, which conserves volume. Apart from the timestepping method, the model formulation is roughly the same as that used in Allison et al. (2010, 2011), although details of, for example, wind stress forcing are altered to suit the problem at hand. The model uses spherical polar coordinates and velocity boundary conditions are applied using ghost points. Ghost points can lead to the underestimation of viscous stresses near boundaries (Adcroft & Marshall, 1998). However, our emphasis here is on traceability to previous work and simplicity.

The wind forcing is given by the following simple analytic expression

$$\tau_x = \begin{cases} 0 & \text{if } \phi > -39°, \\ \tau_0 \cos^2(\pi(\phi + 54.5)/30) & \text{if } -69.5° \le \phi \le -39.5°, \\ 0 & \text{if } \phi < -70°, \end{cases} \qquad (3)$$

$$\tau_y = 0,$$

where $\boldsymbol{\tau} = (\tau_x, \tau_y)$, τ_0 is the peak wind stress and ϕ is the latitude in degrees. This places the peak wind at 54.5°S and makes a cosine-bell 30° wide (allowing for grid staggering). This ensures that the wind stress is zero within the region of deep water formation (if present), to prevent any numerical issues, and to the north of the southern tip of "Africa." The shape of this idealized wind profile is shown in the left-hand panel of Figure 2. Restricting the applied wind stress to just the Southern Ocean ensures that the change in circumpolar transport is visible when the "Antipodes" (see below) is large and the flow is weak. If wind stress to the north of 40°S was included, this would introduce a series of gyres to the circulation, as determined by the curl of the wind stress. This would obscure the circumpolar flow and make our results harder to interpret.

The idealized continental geometry is shown in Figure 2. It consists of two ocean basins connected by two partial barriers to the flow. The southern boundary is at 74°S and the northern boundary is at 65°N. This configuration is similar to that used by Allison et al. (2010, 2011), with the addition of a second ocean basin and an accompanying second barrier to the flow.

The left-hand basin in Figure 2 is 120° wide in longitude; we identify this basin with, and refer to it as, the Indo-Pacific basin. The right-hand basin is 60° wide in longitude; we identify this basin with, and refer to it as, the Atlantic basin. The two partial barriers between the basins are both 16° wide. The barrier to the west of the Indo-Pacific basin begins at 38°S and extends northwards to the northern boundary. This barrier represents the continental landmass made up by Europe, Africa, and Asia. The barrier to the west of the Atlantic basin begins at 64°S

and extends northwards to the northern boundary. This barrier represents the landmass made up of North and South America and the narrower constriction between it and the southern boundary represents Drake Passage.

The light gray-shaded region in Figure 2 is the "Antipodes," a landmass added to the southern boundary to act as our model's analog of Australia, Tasmania, and Zealandia. This landmass is always 20° wide in longitude, which is the scaled width of the modern Antipodes, taking into account the reduced width of the model's Indo-Pacific basin. The latitudinal extent of the Antipodean landmass varies between experiments, as does its attachment to the southern boundary, as described in Sections 3.2 and 3.3.

There are a total of 132 numerical experiments, divided into pairs with and without deep water formation that are otherwise the same, for a total of 68 in each set. The first such pair are the reference experiments without an Antipodean landmass. These are discussed in Section 3.1 as controls for how the Antipodes then impacts the circulation. Of the remaining experiments, 35 pairs (70 experiments) have an Antipodean landmass attached to the southern boundary and its meridional extent is increased by 4° between each experimental pair. The final pair of experiments have the northern and southern boundary connected by a landmass 140° in extent, such that there is no longer a zonal channel between them at any latitude. These experiments are discussed in Section 3.2. The final 30 pairs (60 experiments) have an Antipodean landmass of meridional extent 24° that is separated from the southern boundary and gradually moves northwards (representing the Tasman Seaway). In between each pair, the landmass is moved 4° farther north. These experiments are discussed in Section 3.3.

Each numerical experiment is run for sufficiently long to reach its final equilibrium. We define equilibrium as being attained when the absolute and relative change between circumpolar transport values 30 days apart are less than 2×10^{-5} Sv and 1×10^{-6}, respectively. The absolute change is the difference between the two transport values and the relative change is the absolute change divided by the most recent value. This can take anywhere from 2,000 to 30,000 model years. A single experiment without deep water formation does not meet these criteria. This experiment has its Antipodean land mass extending from the southern to the northern boundary and has a total circumpolar transport of only -0.0553 Sv; it is the only experiment to have a net westward circumpolar transport. The absolute change in transport for this experiment is only 0.01×10^{-5} Sv, which is the smallest of all the experiments, and so we deem that this is sufficiently spun up for our purposes.

2.2. Transport Streamfunction and Transport Potential

Typically a simple model like the one used here can have its flow described with a transport, or barotropic, streamfunction, which is a convenient way to diagnose flow direction and speed for the depth-integrated flow. Contours of a streamfunction are parallel to the flow and changes in speed are seen as contours coming closer together (acceleration) or further apart (deceleration). We name the diagnostic we calculate here as the transport streamfunction since it has units of Sverdrups and the process of its calculation is more involved than is typical for the barotropic streamfunction.

The transport streamfunction described above would be defined as

$$h(\mathbf{u} + \mathbf{u}^*) = \mathbf{k} \times \nabla\psi, \tag{4}$$

where $h\mathbf{u}^* = -\kappa_{GM}\nabla h$ is the bolus velocity due to the (parameterized) eddy field and ψ is the streamfunction. ψ is then obtained by integration of $h(u + u^*)$, the zonal thickness transport, southwards from the northern boundary. This definition relies upon the (steady state) thickness transport being non-divergent and so conserving volume, or, equivalently due to fixed surface area, the thickness itself. However, as can be seen in Equation 2, this is not the case for our model due to the inclusion of diapycnal diffusion and deep water formation near the southern boundary. For the model to conserve volume, the right-hand side of Equation 2 would have to be zero. This can be achieved by setting κ_v and γ to zero. The inclusion of thickness diffusion as a form of the Gent and McWilliams (1990) parameterization does not prevent the model from conserving volume because it has been written as the divergence of a flux and it is required to obey the no normal flow/flux condition at solid boundaries. This means that it can be incorporated into the divergence of thickness fluxes on the left-hand side.

To properly account for the presence of divergent forcing in Equation 2, the thickness transport must be described using a combination of a transport streamfunction and a transport potential. This is defined by

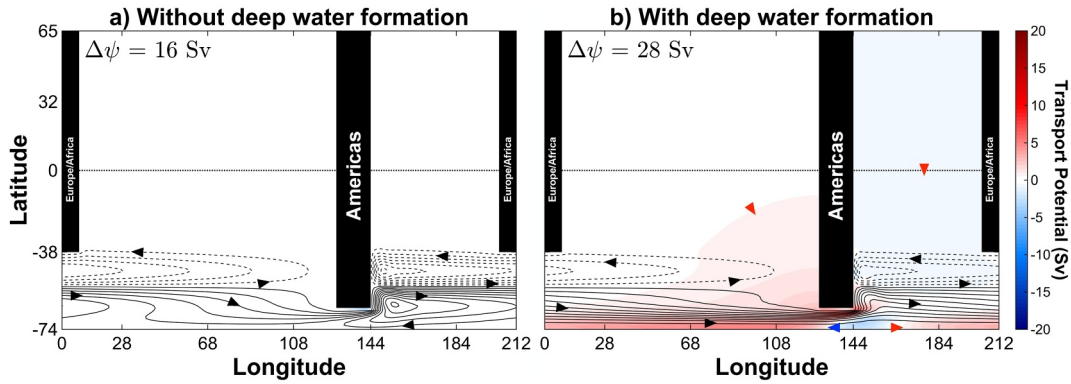

Figure 3. Transport streamfunction for the reference experiments (a) without deep water formation and (b) with deep water formation. Black regions are land. Positive transport streamfunction (clockwise circulation) is solid contours, negative transport streamfunction (anticlockwise circulation) is dotted contours. Color is the transport potential (upgradient flow). Note that the contour interval ($\Delta\psi$) for the transport streamfunction differs in order to allow a visual comparison of the flow structure. Black arrow heads indicate the direction of the flow along contours of transport streamfunction. Red/blue arrow heads indicate the direction of flow perpendicular to contours of transport potential.

$$h(\mathbf{u}+\mathbf{u}^*) = \mathbf{k}\times\nabla\psi + \nabla\chi, \tag{5}$$

where χ is the transport potential. Like the transport streamfunction, ψ, the transport potential has units of Sverdrups.

The transport potential represents the portion of the flow that doesn't conserve volume/thickness and the streamfunction represents the portion of the flow that does. The portion of the flow described by the transport potential is directed across contours of χ, from low to high values, and flows from sources of thickness toward sinks of the same. In Equation 2, vertical diffusion acts as a source of thickness, since it tends to deepen thin layers of fluid faster, and the deep water formation acts as a sink by reducing h near the southern boundary. Therefore, we can broadly expect the portion of the flow represented by the transport potential to flow toward where the deep water formation is strongest. In contrast, the flow described by the transport streamfunction is along contours of ψ with high values to the right. As such, this component of the flow is clockwise around local maxima and anti-clockwise around local minima. In the event that flow is both nondivergent (conserves h) and irrotational ($\xi = 0$), ψ or χ will describe the flow equally well and only one is required; whichever is calculated second would be zero. Nevertheless, if both are calculated, contours of the two will cross each other at right angles.

To obtain the transport streamfunction and transport potential in Figure 3, we use a Helmholtz decomposition (see, e.g., Jayne & Marotzke, 2002; Marshall & Pillar, 2011). Beginning from Equation 5, it can be seen that

$$\nabla\cdot\{h(\mathbf{u}+\mathbf{u}^*)\} = \nabla^2\chi. \tag{6}$$

χ can then be obtained using any of the many iterative solving techniques applicable to what is essentially Poisson's equation. We choose to use the conjugate gradient method to solve for χ. The boundary condition of no normal gradient is applied implicitly to χ during the iteration process. Once χ is known, its contribution to the zonal thickness transport is calculated and removed from $h(u+u^*)$. The remainder is the nondivergent part of the thickness transport that can be integrated meridionally to give ψ, which has its boundary condition of a constant value along each contiguous boundary applied automatically by our solution procedure. This follows the solution method as laid out by Pillar (2013), to which the interested reader is referred.

Whilst we choose to show the structure of the flow using the transport streamfunction and transport potential, it is important to remember that the total velocity is made up of contributions from both. This means that the direction of the total flow is at a slight angle to the contours of streamfunction, rather than strictly along them. When reporting the transport through the model's "Drake Passage," we integrate the full velocity field to avoid under-/over-reporting the volume of fluid passing through the constriction and therefore around the model's "Antarctica."

In doing so, we neglect the contribution of the bolus velocity, $h\mathbf{u}^*$, to the zonal transport to better reflect the transport values reported in the literature.

2.3. Potential Vorticity

Potential vorticity (PV) is a useful dynamical concept that can be used to understand complex aspects of ocean circulation in a relatively simple way. Much of this is due to PV being largely conserved below the mixed layer, that is, the right-hand side of its governing equation is (close to) zero once fluid parcels are isolated from surface forcing. Within the mixed layer, surface wind and temperature/salinity forcing are strong, which can lead to modification of a fluid parcel's PV. The exact form of the PV equation depends upon the governing equations themselves, and so must first be derived. In the case of our reduced gravity formulation, the form of the PV equation is well established (see, e.g., Klinger & Haine, 2019; Vallis, 2017). Note that, in this context, there is little difference between the reduced gravity and shallow water equations.

Neglecting forcing or dissipation on the right-hand sides of Equations 1 and 2, the reduced gravity PV equation is given by

$$\frac{D}{Dt}\left(\frac{\xi + f}{h}\right) = 0, \tag{7}$$

where $D/Dt = \partial/\partial t + (\mathbf{u} \cdot \nabla)$ is the material derivative. In the limit that $\xi \ll f$, that is, that the Rossby number is small, a condition which prevails over much of the ocean, this reduces to

$$\frac{D}{Dt}\left(\frac{f}{h}\right) \approx 0. \tag{8}$$

This is a deceptively simple statement that a fluid parcel will move in such a way as to conserve its value of f/h, as long as forcing and dissipation are weak/zero. When bathymetry is present, which we are enclosing in our inactive bottom layer, this allows us to understand how and where the flow will be strongly steered by the bathymetry. For example, in the modern ocean the path of the ACC is heavily constrained by bathymetric features, such as Kerguelan Plateau or the South-East Indian Ridge, and the steep bathymetry in Drake Passage (see, e.g., Mazloff et al., 2010). Many of these features can be seen in maps of the modern day ocean's f/h contours (see, e.g., Figure 11 of Marshall (2011)). In the simple channel model experiments of Munday et al. (2015) this can be seen in the strong steering of the flow by the bathymetric ridge, which results in large north-south excursions of the flow. In contrast, in the flat bottomed experiments of, for example, Munday et al. (2015) or Abernathey et al. (2011) the mean flow is zonally symmetric, since there is no bathymetry to steer it.

PV is also of great facility when considering wind-driven gyres. In the interior of the gyre, the curl of the wind is able to modify a fluid parcel's value of f/h. This allows them to migrate meridionally, due to Sverdrup transport, and cross contours of f/h. In the western boundary current region a different dynamical balance prevails, which allows the western boundary current to close the circulation of the gyre. In the early examples of Stommel (1948) and Munk (1950), bottom friction and viscosity are able to modify the PV and facilitate meridional motion, that is, the crossing of f/h contours. These terms are largest in the western boundary region, where velocities and velocity gradients are much higher than in the Sverdrup balance-dominated interior. In the case of a sloping western boundary current, a modified balance takes place and motion is unlikely to be purely meridional (Jackson et al., 2006).

In the case of our simple reduced gravity model, PV remains a useful concept. The enclosure of the bottom bathymetry in the inactive layer frees our solution from strong bottom steering. However, the model's contours of f/h will still intersect our idealized continents. This implies that, in the absence of forcing and dissipation, there would be no flow, since the boundary condition of no normal flow at the continent would project along the f/h contour. This is an example of the profound influence of boundary conditions, both in the sense that it is the no normal flow condition that would prevent flow, but also that the addition of forcing and dissipation would free us from this constraint. In our simple solutions, this allows us to infer, for example, which processes may be responsible for modifying the PV at locations where f/h contours are crossed and how the model dynamics allow the flow's value of f/h to be altered to allow this flow.

3. Model Results

3.1. Reference Experiment

The reference experiment pair have the geometry and forcing described in Section 2.1. The southern boundary has no Antipodean landmass, and no island in the Indo-Pacific basin. The steady state transport streamfunction and transport potential for the reference experiment are shown in Figure 3 both with and without southern deep water formation, which highlights the impact of this physical process. Figure 3, and those that follow, shows the transport streamfunction as black contours with black arrowheads showing the direction of flow. Dashed black contours are in regions of negative transport streamfunction, indicating that the flow circulates anti-clockwise around the local minima. Transport potential is shown as blue-white-red shading for negative-positive values. Flow is along gradients of transport streamfunction from negative to positive values, as indicated by the blue and/or red arrowheads. Transport potential is shown for all experiments, although for those with no deep water formation values are very small and close to zero. In order to improve the visual comparison of the flow structure, the contour interval of the transport streamfunction varies between experiments. This is reported as $\Delta\psi$ in the top left of each figure panel.

For the reference case without deep water formation, Figure 3a, an 82.3 Sv circumpolar current flows around Antartica. The model ACC undergoes a significant excursion north of Drake Passage latitudes, as with the modern ACC, with its axis being roughly aligned with the peak in the wind stress jet (at 54.5°S). The curl in the wind stress to the north of the model's ACC also drives a significant "supergyre" (Speich et al., 2007), with a transport of ∼108 Sv, which spans both basins north of the model's ACC to the southern limit of the model's Cape Agulhas. The curl of the wind also leads to a gyre embedded in the flow south of the model's ACC core. This is despite the lack of a continent within Drake Passage latitudes. In the framework of PV, briefly laid out in Section 2.3, the curl of the wind leads to a Sverdrup transport and drives flow across f/h contours in the interior of the gyre. This flow is relatively slow. In the western boundary regions, the southwards/northwards Sverdrup transport is returned northwards/southwards by a western boundary current. Given the viscous/diffusive nature of our reduced gravity model, the meridional motion will be facilitated by viscous modification of PV, which allows the fluid parcels to cross contours of f/h.

There is little flow structure, or variation in the active layer thickness, north of the edge of the supergyre due to the lack of wind forcing at higher latitudes. Broadly speaking, the reference experiment is similar to the experiments of Allison et al. (2010, 2011), at least for those in which their wind stress was placed toward the southern boundary.

The layer thickness does not outcrop near the southern boundary in the reference case without deep water formation. There is a tilt to the interface between the active layer and motionless abyss, which is a result of the balance between the applied wind stress and the parameterized eddies. This naturally leads to a thinner active layer near the southern boundary with the difference in layer thickness across the Southern Ocean being ∼120 m. This remains insufficient to cause the active layer to outcrop at the surface. Changing the model forcing or parameters could alter this situation. For example, strengthening the surface wind stress would lead to a steeper tilt of the pycnocline whilst increasing κ_{GM} would flatten it out. Such changes would make it more/less likely that the pycnocline outcrops.

To the north, the large surface area of the two basins allows the diapycnal diffusion to thicken the active layer until it reaches values that are excessively deep for the modern ocean. In part, this is due to the lack of northern deep water formation. Northern deep water formation, which is included in the theoretical formulation of Gnanadesikan (1999), would thin the layer and, depending upon the length of the restoring timescale and depth, reduce it to a more realistic value and oppose the diapycnal diffusion. In doing so, it might also lead to outcropping near the southern boundary, if the reduced active layer thickness was small enough.

The addition of deep water formation near the southern boundary in Figure 3b increases the circumpolar transport of the model's ACC to 270 Sv, which exceeds observational estimates of the modern ACC. This is due to the much stronger meridional gradient in layer thickness caused by the deep water formation reducing it to 10 m near the southern boundary. In addition, the layer thickness in the northern basins is >2,500 m, which is considerably deeper than the ∼800 m typically observed. As with the reference experiment without deep water formation, this is partly because the model lacks northern deep water formation, which would drain the layer thickness and reduce the circumpolar transport. The large change in layer thickness across the Southern Ocean drives a

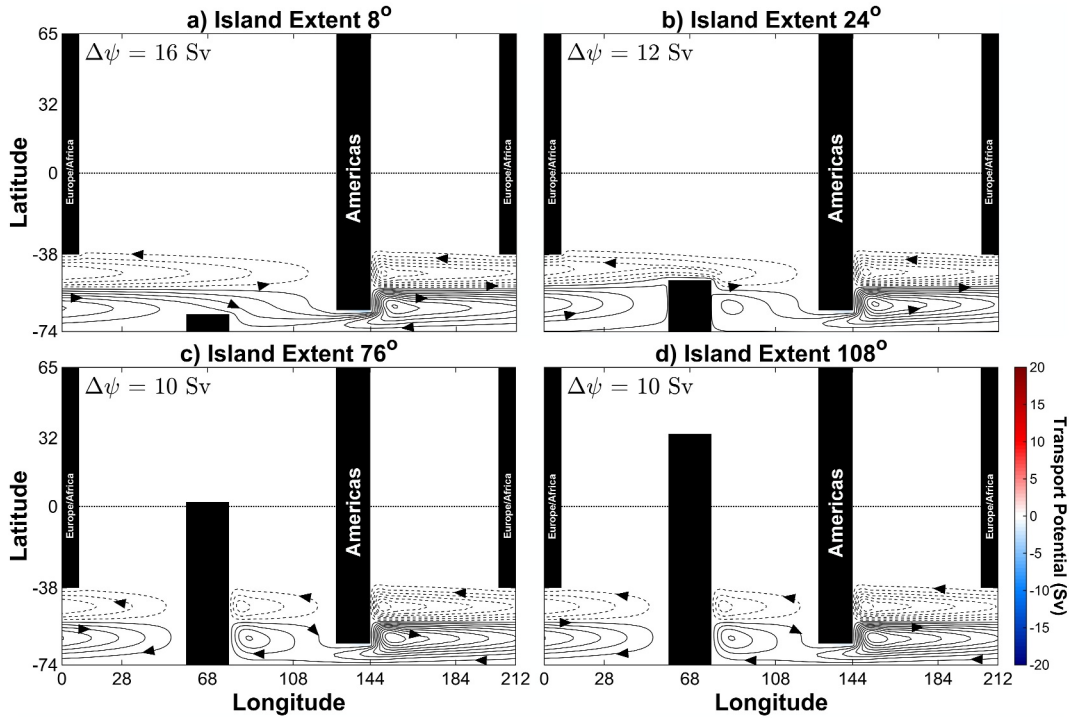

Figure 4. Transport streamfunction for a selection of closed seaway experiments without deep water formation (a) island extent 8°, (b) island extent 24°, (c) island extent 76°, and (d) island extent 108°. Black regions are land. Positive transport streamfunction (clockwise circulation) is solid contours, negative transport streamfunction (anticlockwise circulation) is dotted contours. Color is the transport potential (upgradient flow). Note that the contour interval ($\Delta\psi$) for the transport streamfunction differs in order to allow a visual comparison of the flow structure. Black arrow heads indicate the direction of the flow along contours of transport streamfunction. Red/blue arrow heads indicate the direction of flow perpendicular to contours of transport potential.

concomitantly stronger geostrophic zonal flow eastwards than the reference experiment without deep water formation. The supergyre also increases in transport from 108 to 122 Sv (counterclockwise). This is because the enhancement in the meridional gradient of layer thickness persists across most of the model's Southern Ocean, leading to higher velocities. Note that no other parameters or forcing (other than the timestep) has been changed between Figures 3a and 3b; the change in circumpolar transport can be directly attributed to initiation of deep water formation in Figure 3b.

As well as increasing the circumpolar transport, the initiation of deep water formation also introduces a much stronger divergent component of the flow in Figure 3b. Diapycnal water mass transformation acts to increase layer thickness, largely north of the model's Southern Ocean. However, it remains weak in both reference experiments. The introduction of deep water formation reduces the layer thickness near the southern boundary from ∼250–10 m. This loss of volume is fed by a divergent flow that is largely southwards, since the flow is upgradient with respect to χ, as shown by the color-shading in Figure 3b. This supplies water to the deep water formation region and acts to offset the loss of volume due to deep water formation. Broadly speaking, the divergent part of the flow is stronger in the Pacific basin, due largely to its width. In the PV framework of Section 2.3, the deep water formation acts as a sink/source of PV on the right-hand side of Equation 8. This allows the non-divergent flow to cross f/h contours and provide fluid to the southern boundary of the model.

3.2. Closed Seaway

In the set of experiments discussed in this Section, the Antipodean landmass remains attached to the southern boundary and its meridional extent is gradually increased. Representative examples of transport streamfunction and transport potential for experiments with an Antipodean landmass of 8°, 24°, 76°, and 108° meridional extent are shown in Figure 4. None of these experiments include deep water formation.

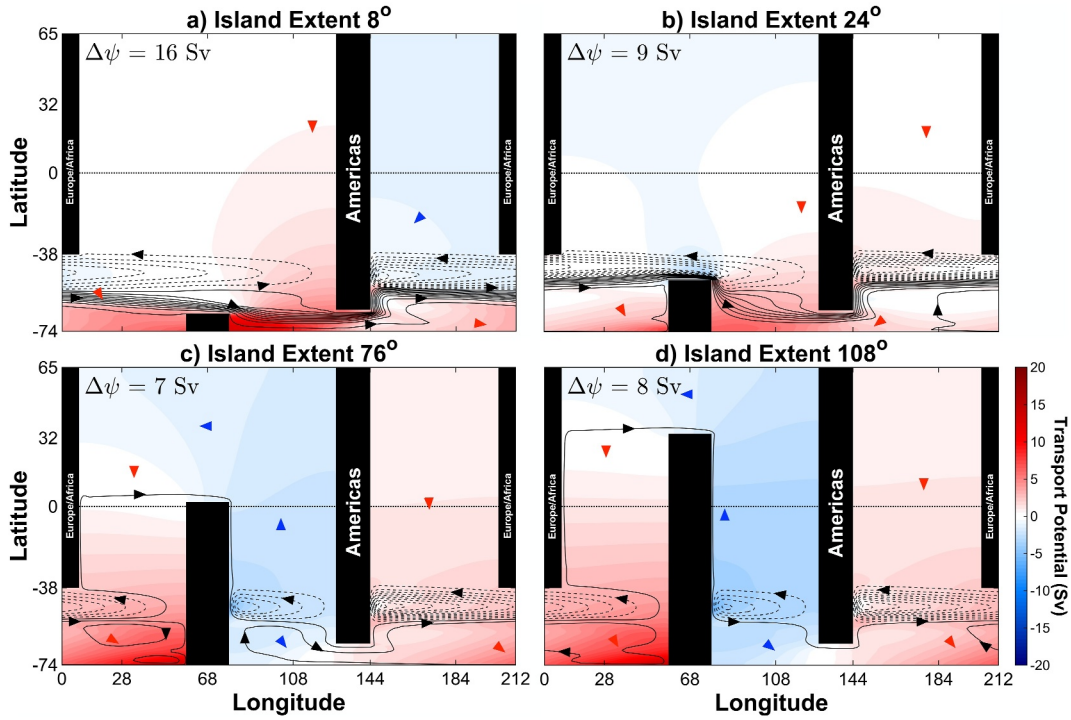

Figure 5. Transport streamfunction for a selection of closed seaway experiments with deep water formation (a) island extent 8°, (b) island extent 24°, (c) island extent 76° and (d) island extent 108°. Black regions are land. Positive transport streamfunction (clockwise circulation) is solid contours, negative transport streamfunction (anticlockwise circulation) is dotted contours. Color is the transport potential (upgradient flow). Note that the contour interval ($\Delta\psi$) for the transport streamfunction differs in order to allow a visual comparison of the flow structure. Black arrow heads indicate the direction of the flow along contours of transport streamfunction. Red/blue arrow heads indicate the direction of flow perpendicular to contours of transport potential.

Figure 4 demonstrates that as the Antipodean landmass grows, and gradually divides the southern section of the Indo-Pacific into two, it disrupts the path of the model ACC. Initially this provides an extra source of friction near the southern boundary (Figure 4a), reducing the magnitude of, but still allowing, circumpolar transport. The continued growth of the landmass goes on to disrupt the circulation of the supergyre. For landmasses of extent greater than about 36°, such that the northern tip is at the same latitude as the tip of Africa, the supergyre breaks cleanly in two with separate gyres in the Atlantic/western Indo-Pacific and eastern Indo-Pacific. At this point the circumpolar transport has also been reduced to near zero (see below). The Southern Ocean is now occupied by a series of wind-driven gyres propped up by the landmasses and a new clockwise supergyre takes up the rest of the Southern Ocean.

The introduction of deep water formation near the southern boundary acts to change the character of experiments with an attached Antipodean landmass in similar ways to in the reference experiments. As with Figure 4a, with a small Antipodean landmass an extra source of friction is introduced and the circumpolar transport drops slightly (Figure 5a). However, as the landmass grows in Figure 5b the axis of the ACC is pushed northwards, rather than flow being completely blocked. Due to the steep meridional gradient in layer thickness, a geostrophic zonal flow is still supported. Even when the Antipodean landmass reaches the latitude of the model's Cape Agulhas, several tens of Sverdrups are able to circulate around its Southern Ocean. When the tip of the Antipodes extends beyond the Equator, circumpolar contours of streamfunction still exist, creating a circumpolar transport of ∼10 Sv. For the flow to cross the Equator, it must change its sign of f/h. Friction with the sidewalls provides the means to do this and promotes fluid flow across the Equator. At this point the circumpolar flow exists as a series of meridional/western boundary layers connected by piece-wise quasi-zonal flow, much like the model of Webb (1993) and the linear models of the ACC reviewed by LaCasce and Isachsen (2010).

For an island extent of 140° the divided supergyre in the northern half of the model's Southern Ocean is very similar both with and without deep water formation, see Figure 6. Without deep water formation there is also a

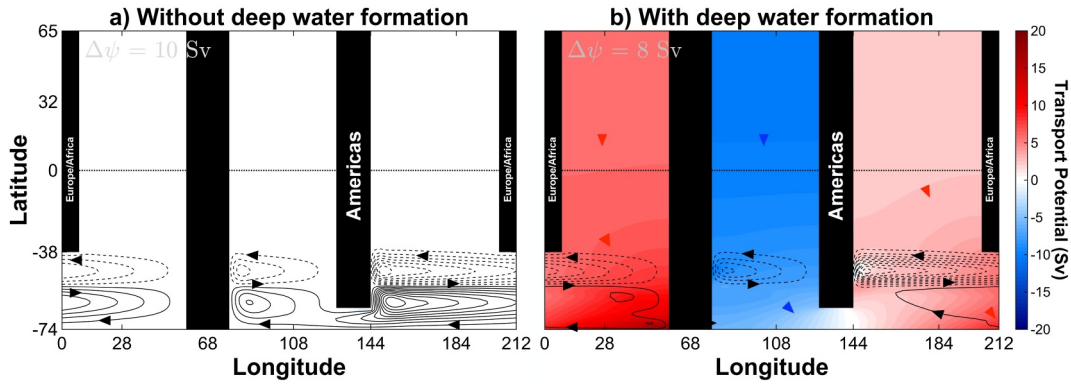

Figure 6. Transport streamfunction for the experiments with an island extent of 140° (a) without deep water formation and (b) with deep water formation. Black regions are land. Positive transport streamfunction (clockwise circulation) is solid contours, negative transport streamfunction (anticlockwise circulation) is dotted contours. Color is the transport potential (upgradient flow). Note that the contour interval ($\Delta\psi$) for the transport streamfunction differs in order to allow a visual comparison of the flow structure. Black arrow heads indicate the direction of the flow along contours of transport streamfunction. Red/blue arrow heads indicate the direction of flow perpendicular to contours of transport potential.

supergyre in the southern half of the model's Southern Ocean. However, when deep water formation is turned on, this supergyre is disrupted by the strong meridional gradient in layer thickness. The result is very weak transport streamfunction values. The divergent flow, as shown by the transport potential, is notably stronger in Figure 6b than in Figure 5d (as shown by the strength of the color shading). This is an indication of stronger flow into the deep water formation region in Figure 6b. The circumpolar transport without deep water formation is slightly westward (negative) and with deep water formation it remains eastward (positive), albeit only 4.5 Sv. These non-zero transports are slightly surprising, given the barrier extending over the full meridional extent of the model's Pacific and they are not circumpolar as a result. Rather they are a net flow through the model's Drake Passage as a result of the divergent nature of Equation 2 due to the inclusion of diapycnal diffusion and deep water formation. If these processes provide a larger sink or source of h in one of the basins, then a flow between them will be established in order for the model to reach equilibrium. Close examination of the transport streamfunction shows that it continues to respect no net flow through the open gateways, as it represents the non-divergent component of the flow. It is the transport potential that supplies the net flow, consistent with it representing the divergent flow.

The steady state circumpolar transport for all experiments in which the Antipodean landmass is attached to the southern boundary is summarized in Figure 7a. In the absence of deep water formation (red line in Figure 7a) the addition of a small Antipodes causes a decrease in circumpolar transport. The circumpolar transport then holds roughly constant until the Antipodes is >12° in extent. This can be attributed to increased friction with the southern boundary, due to a slightly longer perimeter, and the addition of a form stress/pressure difference across the landmass. Bottom form stress is the primary sink of zonal momentum for the real Southern Ocean, although continental form stress can play a role for obstructed ACC's as here (Munday et al., 2015). Once the Antipodes exceeds this extent, the circumpolar transport decreases smoothly to almost zero as the path of the circumpolar current becomes increasingly obstructed. The circumpolar transport cannot recover once this has taken place and when the Antipodes extends all the way to the northern boundary (Figure 6a) the transport is actually slightly negative (westward).

The addition of deep water formation increases the circumpolar transport of the reference case from 82.3 to 270.0 Sv (blue line in Figure 7a). The decrease with the addition of a small Antipodes is very rapid, with the transport reaching 132.8 Sv for an Antipodes 12° in extent. The subsequent decrease in circumpolar transport as the Antipodes continues to grow persists across all the experiments. Even when the Antipodes extends across the Equator the circumpolar transport is 11.6 Sv. This is because the deep water formation continues to enforce a strong meridional gradient in layer thickness, which contributes to the geostrophic zonal flow. The formation of meridional boundary layers is then able to funnel fluid across the Equator by viscous modification of the fluid's PV, which allows flow to cross f/h contours. Even when the Antipodes extends all the way to the northern boundary the transport remains slightly eastward (positive), in contrast to the case without deep water formation. This is due to preferential deep water formation taking place in the western Indo-Pacific and the Atlantic due to

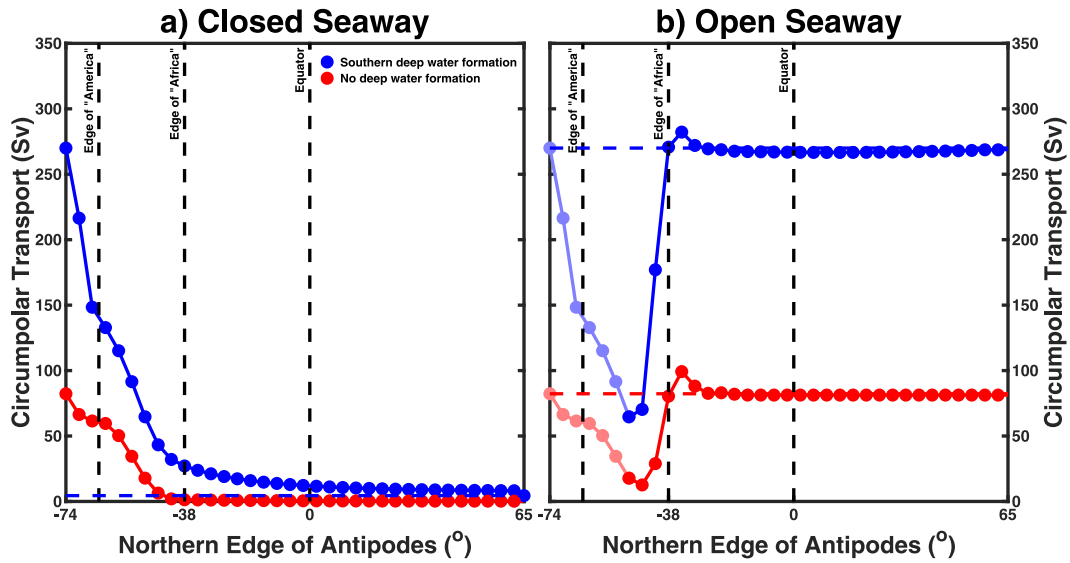

Figure 7. (a) Circumpolar transport as a function of the position of the Antipodean landmasses northern edge. −74° corresponds to the reference case with no island, 65° corresponds to the island extending to the northern boundary. (b) Circumpolar transport as a function of the position of the Antipodean landmasses northern edge. The island land mass is 24° in latitude; −50° corresponds to the island being attached to the southern boundary, that is, Island Extent of 24° in Figures 4b and 5b. The desaturated points in (b) are the first six points from (a).

their combined width. Water must then flow from the eastern Indo-Pacific, via Drake Passage, to compensate the lost layer thickness due to the restoring. This creates an eastward (positive) Drake Passage transport.

3.3. Open Seaway

In the set of experiments discussed in this Section, an Antipodean landmass of meridional extent 24° is separated from the southern boundary and gradually moved northwards (representing the Tasmanian Seaway). Experiments with and without deep water formation are performed and are shown in Figures 8 and 9, respectively.

In the absence of deep water formation the change in basin topology due to an Antipodean landmass of 24° meridional extent breaking away from the southern boundary makes little difference to the circumpolar transport or the qualitative features of the circulation (cf. Figures 4b and 8a). The Southern Ocean is still dominated by a pair of supergyres, although it is only the southernmost that is split completely in two by the Antipodes. When the Antipodes is 8° away from the southern boundary in Figure 8b, the circumpolar flow shifts to the southern side of the Antipodes and decreases slightly in terms of circumpolar transport at the model Drake Passage. As the Antipodes continues to move northwards the circumpolar transport is able to increase due to the removal of a large obstacle to the flow. Once the Antipodes is clear of the latitudes of significant circumpolar flow, any further movement northwards does little to the transport. As demonstrated in Figures 8c and 8d, there is also little change in the structure and path of the streamlines.

The divergent part of the flow, as shown by the color shading for χ, remains weak in Figure 8, just as in Figure 4, and is concentrated around the exit from Drake Passage. Here the total flow is strong and this sharp turn leads to large horizontal divergence and thus large gradients in χ. Despite this, the flow remains largely non-divergent, as shown by the contours of ψ and largely constant values of χ elsewhere in the domain.

The initiation of deep water formation in Figure 9 leads to a strengthening of circumpolar transport for all seaway extents. As the island migrates away from the southern boundary, the restoration of the layer thickness to $h^\star$ quickly leads to the majority of its transport occurring on its southern side. With only 4° between the southern boundary and the southern edge of the landmass (Figure 9a), approximately 2/3 of the total transport of the current passes to the south of the landmass. Once the island's southern boundary is north of about 50°S, the presence of the island has little further impact upon the model ACC, as shown in Figure 9c for the case of the seaway being the same width as the island. However, the supergyre continues to be disrupted.

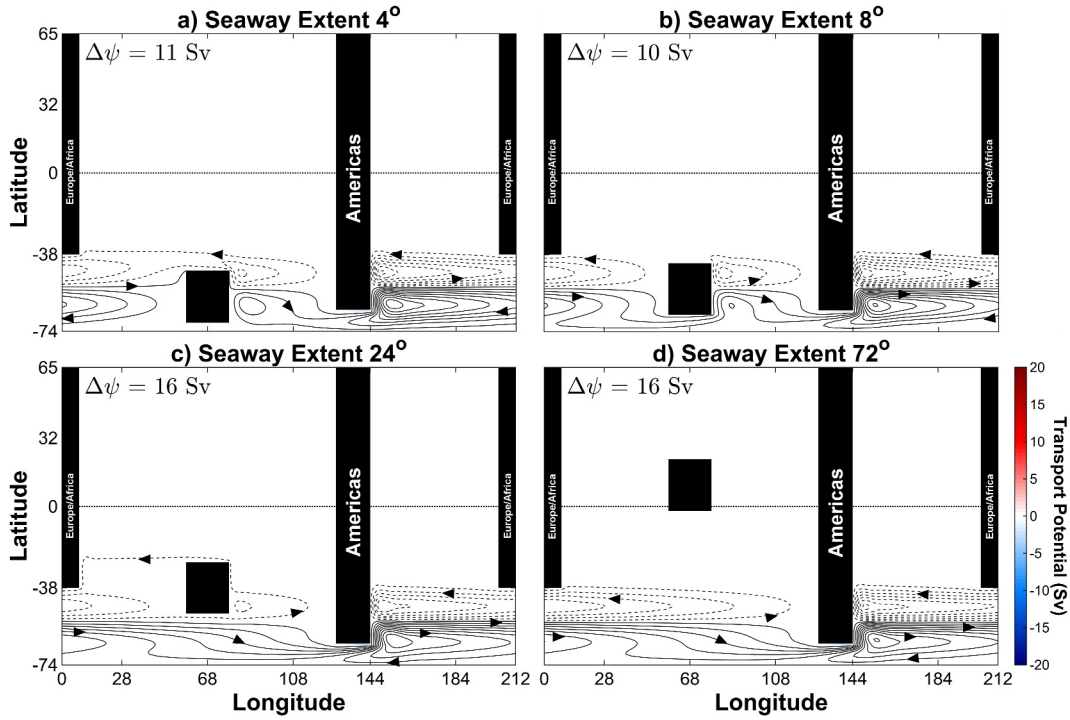

Figure 8. Transport streamfunction for a selection of open seaway experiments without deep water formation (a) seaway extent 24°, (b) seaway extent 48°, (c) seaway extent 72° and (d) seaway extent 96°. Black regions are land. Positive transport streamfunction (clockwise circulation) is solid contours, negative transport streamfunction (anticlockwise circulation) is dotted contours. Color is the transport potential (upgradient flow). Note that the contour interval ($\Delta\psi$) for the transport streamfunction differs in order to allow a visual comparison of the flow structure. Black arrow heads indicate the direction of the flow along contours of transport streamfunction. Red/blue arrow heads indicate the direction of flow perpendicular to contours of transport potential.

The steady state circumpolar transport for all experiments in which a 24° Antipodean landmass is detached from the southern boundary and moved northwards is summarized in Figure 7b. We repeat the first six points from Figure 7a, as the Antipodes is growing to 24° in extent, to highlight how the subsequent detachment of the Antipodes changes the downwards trend.

When the Antipodes is first detached (4° seaway), the circumpolar transport does not increase straight away without deep water formation. In fact, it drops to roughly the same level as growing the Antipodes such that its northern edge is at the same latitude (28° island). However, subsequent widening of the seaway leads to rapid growth of the circumpolar transport. Both with and without deep water formation the circumpolar transport is on par with that of the reference simulation when the northern edge of the detached Antipodes is level with the southern edge of "Africa." The circumpolar transport actually overshoots slightly when the Antipodes is moved a further 4° northwards before decreasing to match the reference case once more.

4. Summary and Discussion

The timeframe in which Drake Passage opened between Cape Horn and the Antarctic continent is poorly constrained (e.g., Barker & Thomas, 2004). In contrast, the opening of the Tasman Gateway is relatively well-dated to between 35.5 and 30 Ma (Barker et al., 2007). In the past, the literature has sometimes assumed that a belt of open circumpolar latitudes is a prerequisite for the formation of a circumpolar current. However, recent theoretical advances regarding the path and transport of the ACC have shown that it can migrate several thousand kilometers north of any open circumpolar latitude band in order to follow the wind forcing (Allison et al., 2010; Marshall et al., 2016). This suggests that in deep paleo-time, it may have been possible for a considerable circumpolar current to have formed prior to the opening of the Tasman Gateway if Drake Passage was already open. The model of Sauermilch et al. (2021) does not produce circumpolar flow when the Tasman Gateway is closed and the domain extended to the Equator. However, with Eocene temperature and salinity forcing, the density gradient

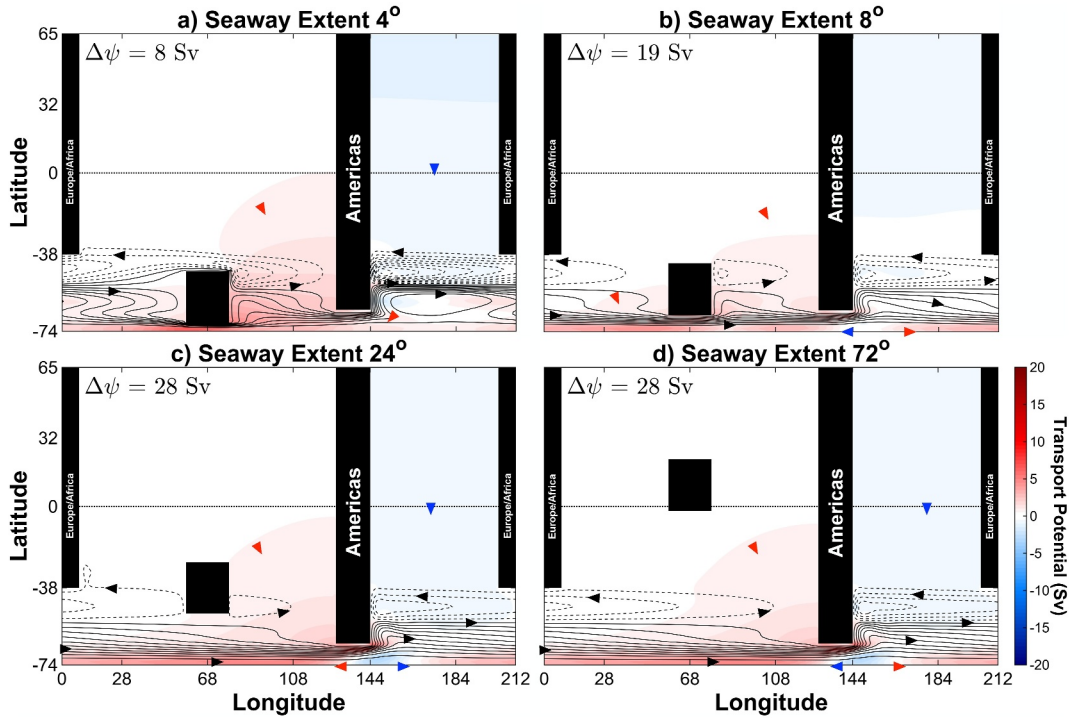

Figure 9. Transport streamfunction for a selection of open seaway experiments with deep water formation (a) seaway extent 24°, (b) seaway extent 48°, (c) seaway extent 72°, and (d) seaway extent 96°. Black regions are land. Positive transport streamfunction (clockwise circulation) is solid contours, negative transport streamfunction (anticlockwise circulation) is dotted contours. Color is the transport potential (upgradient flow). Note that the contour interval ($\Delta\psi$) for the transport streamfunction differs in order to allow a visual comparison of the flow structure. Black arrow heads indicate the direction of the flow along contours of transport streamfunction. Red/blue arrow heads indicate the direction of flow perpendicular to contours of transport potential.

across the Southern Ocean remains lower than in the modern world. This leads them to suggest that the initiation, and/or strengthening, of deep water formation due to buoyancy loss may allow for both a stronger circumpolar transport and circumpolar flow with the Tasman Gateway closed. The initiation of deep water formation and increase in the meridional density gradient across the Southern Ocean are key aspects of the development of the proto-ACC toward the modern ACC strength.

Using a simple reduced gravity model with idealized geometry and forcing, we have demonstrated that deep water formation is crucial in setting the circumpolar transport and can potentially elevate it by the relative amount required to go from the lower Eocene to the higher modern value. For large Antipodean landmasses attached to the southern boundary, deep water formation is able to elevate the circumpolar transport to several tens of Sverdrups. Importantly, even with a closed seaway, circumpolar transport is possible due to flow along the north-side of the Antipodean landmass. Deep water formation is even able to allow for some, albeit very small, circumpolar transport when the Antipodes extends beyond the Equator with a series of viscous boundary layers enabling the cross-Equatorial flow.

Considering the plate tectonic framework from the Cretaceous to the early Cenozoic, this scenario may have been possible. According to van de Lagemaat et al. (2021), Drake Passage may have been open during the Cretaceous and closed again later, whilst the Tasman Gateway remained closed until some time in the Eocene (50 Ma, according to e.g., Bijl et al., 2013). During this time period between the Cretaceous and the Eocene, Australia and Antarctica experienced late rifting and ultra-slow seafloor spreading from west to east with the Tasman Gateway being the last section to separate (e.g., Sauermilch et al., 2019). During this tectonic process, the northern section of the Australian plate subsided below the Pacific Plate and, consequently, narrowed the Indonesian Seaway with time. However, previous studies suggest that the Indonesian Seaway still remained a significant width and depth until at least 25 Ma (e.g., Gaina & Müller, 2007). Based on various global paleogeography reconstructions, it can be expected that the latitudes of the northern part of Australia and the southern tip of Africa were not too far off

from each other (with Australia not moving north of the equator). According to our model results, this would allow a certain ACC transport via the Indonesian Seaway and the already open Drake Passage since the Cretaceous, even without deep water formation (see Figure 4). Assuming that deep water formation developed around or even prior to the Eocene (see, e.g., Hague et al., 2012; McKinley et al., 2019; Thomas, 2004; Thomas et al., 2014; Via & Thomas, 2006;), it may be possible that a stronger ACC developed, potentially even before the Tasman Gateway opened, with Australia moving farther north and the Indonesian Seaway narrowing (see Figure 5). It should be noted that our model indicates that only a narrow Tasman Gateway is necessary for circumpolar flow to switch to this southern pathway. This suggests that it would be early in the history of the gateway's tectonic opening and deepening that eastward flow would have begun south of Tasmania.

In the case of a detached Antipodean landmass progressively moved to the north, the transport increases until it is fully recovered to that of the reference experiment. With the smallest separation between landmass and southern boundary considered, 4° or ∼400 km, most of the circumpolar transport is achieved by a strong eastwards flow between the southern boundary and the landmass. Whilst the modern ACC has a volume transport in excess of 130 Sv, a transport of several 10's of Sverdrups would still place such a flow amongst the strongest currents in the modern world. For example, as it flows through Florida Strait, the transport of the Florida Current is 32.2 ± 3.3 Sv (Meinen et al., 2010), which rises to ∼70–75 Sv after separation from Cape Hatteras as the Gulf Stream (Heiderich & Todd, 2020). Other western boundary currents show similar transports, such as the <11 Sv of the Brazil Current between 12°S and 25°S (Imawaki et al., 2013), or the East Australian Current's 22.1 ± 7.5 Sv at 27°S (Sloyan et al., 2016). In this context, the Drake Passage transports of ∼42–44 Sv achieved in the Rupelian geometries of Hill et al. (2013) or in the fully glaciated experiments of Ladant et al. (2014) are quite impressive. It is likely that subsequent changes to thermal forcing would enhance this circumpolar transport toward modern values (Goldner et al., 2014; Lefebvre et al., 2012; Toumoulin et al., 2020; Xing et al., 2023). In addition, in our reduced gravity model the circumpolar transport rapidly recovers to the unobstructed value as the Antipodes separates from the southern boundary and moves northwards, see Figure 3b. This suggests that it would not be necessary for Australia to have reached its modern latitude prior to the inception of a circumpolar current with a volume transport placing it amongst the most powerful currents on Earth, as long as deep water formation has also begun/strengthened in the Southern Ocean.

The changes in the path and transport of the model ACC observed in both sets of experiments have important implications for several aspects of the real ACC. For example, an ACC that migrates to the degree seen here could have a considerably different set of transport properties for heat, salt and other climatically important tracers such as carbon or nutrients. Quantifying the impact of a weak circumpolar current in a warmer climate requires more sophisticated models than a reduced gravity model. Furthermore, mesoscale eddies are of great importance to the circulation of the Southern Ocean, both in terms of the dynamical balance that sets the volume transport of the ACC (Johnson & Bryden, 1989; Munk & Palmén, 1951) and the MOC that accompanies it (Marshall & Radko, 2003). A proper assessment of the changing properties of such circumpolar currents therefore requires the use of an eddy-resolving ocean model at an increase in computing cost of several orders of magnitude. Even in the absence of complex forcing and an increase in the number of vertical levels, reducing the grid spacing of the reduced gravity model used here from 1° to 1/10° would increase the computational cost by a factor of roughly 1,000.

Restoring our reduced gravity model to a shallow thickness near the southern boundary is a very simplified version of deep water formation that acts as a sink of h near the southern boundary. Together with the diapycnal mixing, which is a source of h, it gives the model a simple form of meridional overturning in which water upwells across the thermocline, via diapycnal mixing, and downwells across the thermocline near the southern boundary, via deep water formation. This is a similar framework to that used by Huber and Nof (2006), whose idealized two basin model is mathematically analogous to ours (Gent & McWilliams, 1984) and also includes sinks and sources of mass/volume to represent an overturning circulation. A key difference between the two models is the position of the sinks and sources. These are reversed relative to our model such that the sources of volume are near the southern boundary and the sinks are near the northern boundary in the model of Huber and Nof (2006). As a result of this difference, the two models are simulating the opposite sense of overturning, northwards for Huber and Nof (2006) and southwards for our model. This can be interpreted as the two models representing different aspects of the modern ocean's overturning circulation, with Huber and Nof (2006) representing the northwards flow of NADW in the upper cell and our model representing the southwards return flow at depth of NADW and/or

Antarctic Bottom Water. This is a limitation of both models having only a single active layer, with at least 3 being required to represent both overturning cells in a minimal sense (Shakespeare & Hogg, 2012).

Huber and Nof (2006) demonstrate that the growth of an Australian landmass on their southern boundary acts to reduce the MOC by about 50% when the landmass is sufficiently big so as to just cross the Equator. However, with an Australian landmass that is detached from the southern boundary, but still with its northern boundary at the Equator, the MOC recovers. This is similar to the behavior of the circumpolar transport in the open seaway experiments of Section 3.3. Regardless of the presence of deep water formation, once the southern boundary of the Antipodes is level with the model's African continent, the circumpolar transport has recovered to the control value with no Antipodes. As a result, we might expect the MOC of our model to respond similarly to that of Huber and Nof (2006). However, whilst the circumpolar transport and meridional transport are coupled through the stratification of the ocean (Marshall & Radko, 2003), they are not the same process or circulation. As a result, caution should be exercised in drawing overly strong conclusions regarding the behavior of one based on analysis of the other.

Youngs et al. (2019) use mass fluxes across the interface in their two layer model to impose an overturning. In this way they are able to simulate the northwards overturning of Huber and Nof (2006) and our southwards overturning. This contrasts with our model, which selects a balance between deep water formation (if present), the wind stress, parameterized mesoscale eddies and diapycnal diffusion. This leads to a weak overturning circulation that is capped at about 4 Sv, which is well below that expected for the modern ocean. For the cases with a very large Antipodean land mass reaching the tip of Africa and beyond, the imposition of a large overturning of ∼15 Sv, comparable to the modern ocean and the strongest overturning imposed by Youngs et al. (2019) (factoring in the length of their domain), may alter the transport by a modest amount. In such cases, the transport is already only a few 10's of Sverdrups with deep water formation and very low without. The presence of a stronger overturning than the model naturally achieves may elevate the circumpolar transport toward, and maybe 25% above, the deep water formation line. However, in this case we feel that the large Antipodes would remain a deciding factor leading to a low transport. For cases with a smaller Antipodean landmass, the presence of a strong overturning may be more pronounced and the impact on the circumpolar transport larger, since the circumpolar flow is less impeded by the presence of a continental landmass. When the Antipodes separates from the southern boundary, we would expect broadly the same to be true; the circumpolar transport is elevated above that of the no deep water formation line in Figure 7b and may well be above that of the southern deep water formation experiments.

The simplicity of the reduced gravity model and the idealized nature of the model domain places a number of caveats upon our results. Firstly, the experimental design treats deep water formation as an on/off switch, effectively moving between the two extreme cases of no deep water formation and strong, persistent deep water formation all around Antarctica. Estimates of the Eocene overturning (see below) suggest that there was deep water formation in the Eocene Southern Ocean and so the reality of the scenario suggested by Sauermilch et al. (2021) may have been a strengthening of the processes already taking place. This could have occurred by a geographical broadening of the regions in which deep water formation took place and/or more deep water forming at specific locations. In a scenario involving the strengthening of already present deep water formation, we would consider the increase in circumpolar transport seen here as an extreme limiting case with any actual increase being more moderate.

Secondly, we restrict attention to the steepening of already present isopycnals. In practice, we would expect that an enhanced meridional density gradient would accompany the initiation/strengthening of deep water formation, as highlighted by Lefebvre et al. (2012) and Ladant et al. (2014). It would seem likely that the presence of deep water formation/convection and the generation of steep isopycnals would go hand-in-hand (Xing et al., 2023). In this scenario, the enhancement of the meridional density gradient would reinforce the increasing circumpolar transport due to deep water formation. In our simple reduced gravity formulation, this could be represented by using a smaller g' when there is no deep water formation and a larger g' when deep water formation is turned on. This would increase the difference between the circumpolar transport achieved in each scenario. However, the value of g' we selected is more appropriate to the modern ocean and so we would suggest decreasing the reduced gravity for the case of no deep water formation. This would continue to suggest that the increase in circumpolar transport in our experiments with deep water formation should be considered an extreme limiting case.

A third caveat upon our results is the lack of northern deep water formation. Zhang et al. (2022) considers the most likely scenario for the Eocene ocean would be the absence of deep water formation in the North Atlantic, although particular models may not conform with this MOC structure. In contrast, the modern ocean does have deep water formation in the North Atlantic. The addition of northern deep water formation to the model would thin the active layer and likely reduce the circumpolar transport by reducing the change in layer thickness across the Southern Ocean.

A fourth caveat is the lack of heat/freshwater fluxes at the surface. In the real ocean these fluxes alter the ocean stratification and these can be key to changing the circumpolar transport (Hogg, 2010). In a reduced gravity model, such fluxes can be represented by fluxes of thickness. We have eschewed the use of such fluxes for similar reasons to our use of diapycnal diffusion and layer thickness restoring instead of imposing fluxes of thickness; depending upon other details of each experiment, such fluxes might reduce the local active layer thickness to zero and there are differences between the Eocene and modern surface heat/freshwater flux. In fact, whether the imposition of such fluxes would be considered surface heat/freshwater fluxes or part of the MOC becomes a matter of interpretation, since there is no second layer to move volume to/from as in Youngs et al. (2019).

Finally, an important caveat to our results is that our numerical model does not resolve mesoscale eddies, which are of key importance to the dynamics and circulation of the Southern Ocean (Marshall & Speer, 2012). Mesoscale eddies transport momentum vertically (Ward & Hogg, 2011) and this contributes to the establishment/maintenance of the Southern Ocean's momentum balance between surface wind stress and pressure differences across bathymetric features (Johnson & Bryden, 1989; Munk & Palmén, 1951). The momentum budget of our reduced gravity model is rather different, since its formulation requires the assumption that all of the bathymetry is contained in the motionless abyss. This forgoes a balance between the surface wind stress and bottom form stress. Instead, if the vertically-integrated momentum budget was constructed, the primary balance is likely to be between the surface wind stress and the GM parameterization term in Equation 2 (although the pressure difference across continents likely plays a role, especially with large Antipodean landmasses, see Munday et al., 2015). However, the GM parameterization can be considered to represent the eddy form stresses between isopycnal layers, a point made clear by its geometric interpretation (Mak et al., 2018; Marshall et al., 2012). In this respect, the model's formulation can be interpreted as implying a somewhat more realistic balance; the surface wind stress supplies momentum, which is transferred downwards by the parameterized mesoscale eddies to be balanced by unresolved bottom form stresses in the motionless abyss. One key issue with this interpretation is that there are fundamental differences in the ways that resolved and parameterized eddies respond to changes in forcing, particularly wind forcing, which can change the sensitivity of the circulation to that change in forcing (Abernathey et al., 2011; Hallberg & Gnanadesikan, 2001; Munday et al., 2013; Tansley & Marshall, 2001; Viebahn & Eden, 2010). Whilst we are not concerned with changing wind forcing here, there are large changes in the model's circumpolar transport that is driven by changes in the slope of the active layer thickness across the model's Southern Ocean. If the model resolved mesoscale eddies, it would be a reasonable assumption that this increase in slope would give rise to a stronger eddy field, via baroclinic instability, which would then relax the isopycnal slope and reduce the circumpolar transport. This would affect the experiments with the highest transport the most severely and so reduce the difference between the experiments with and without deep water formation seen in Figure 7. We view the lack of a resolved mesoscale eddy field as the most egregious weakness of our reduced gravity model, although the use of this simple model formulation has allowed for a large number of experiments to be run to equilibrium.

Recent global models, at resolutions requiring the parameterization of mesoscale eddies, differ in their opinion of the overturning regime, and thus bottom water formation site, of the Eocene ocean (e.g., Huber & Nof, 2006; Huber & Sloan, 2001; Sijp et al., 2011). The combined model and proxy analysis of Zhang et al. (2022) suggests that the most likely regime for the early Eocene is one of deep water formation in the Southern ocean, with export northwards, and the absence of deep water formation in the North Atlantic. Even then, there are disagreements between the models that Zhang et al. (2022) analyze as to which Southern Ocean sector houses the deep water formation and the GFDL model also produces deepwater in the North Pacific. These differing overturning regimes may suggest a role for multiple equilibria due to salt advection (Hawkins et al., 2011; Marotzke & Willebrand, 1991; Stommel, 1961) or sea-ice albedo (Budyko, 1969; Ferreira et al., 2011; Sellers, 1969) feedbacks in producing warm equable climates. This can allow for a sudden transition between warm and cold climates with very different circulations (Rose, 2015; Rose et al., 2013). If multiple equilibria were possible under Eocene geometry and forcing, then it may explain the differences between contemporaneous simulations with one

existing in a "warm" state and the other in a "cold" state. Both salt advection and sea-ice albedo are known to be modified by changes in ocean geometry (Ferreira et al., 2011; von der Heydt & Dijkstra, 2008), with sea-ice albedo equilibria being linked to glacial/interglacial cycles (Ferreira et al., 2018). How multiple equilibria might also be modified by the presence of a vigorous mesoscale eddy field is yet to be determined.

Data Availability Statement

The model code used for the numerical experiments is available from Zenodo (Munday, 2022). Model output is available from the Open Science Framework (Munday et al., 2022).

Acknowledgments
DRM was supported by the Natural Environment Research Council (ORCHESTRA, Grant NE/N018095/1). This work used JASMIN, the UK's collaborative data analysis environment (see https://jasmin.ac.uk, Lawrence et al., 2013). Isabel Sauermilch acknowledges funding through the ERC starting Grant n802835 OceaNice. The initial experiments were conducted when DRM was a PDRA at the University of Oxford, supported by the Natural Environment Research Council. This research was partially supported by the Australian Government through the Australian Research Council's Discovery Projects funding scheme (project DP180102280). The authors thank Matthew Huber and three anonymous reviewers whose comments improved the clarity of the paper and led to an improved discussion.

References

Abernathey, R., Marshall, J., & Ferreira, D. (2011). The dependence of Southern Ocean meridional overturning on wind stress. *Journal of Physical Oceanography*, *41*(12), 2261–2278. https://doi.org/10.1175/jpo-d-11-023.1

Adcroft, A., & Marshall, D. (1998). How slippery are piecewise-constant coastlines in numerical ocean models? *Tellus*, *50*(1), 95–108. https://doi.org/10.1034/j.1600-0870.1998.00007.x

Allison, L. C. (2009). Spin-up and adjustment of the Antarctic circumpolar current and global pycnocline. Ph.D. thesis. University of Reading.

Allison, L. C., Johnson, H. L., & Marshall, D. P. (2011). Spin-up and adjustment of the Antarctic Circumpolar Current and global pycnocline. *Journal of Marine Research*, *69*(2), 167–189. https://doi.org/10.1357/002224011798765330

Allison, L. C., Johnson, H. L., Marshall, D. P., & Munday, D. R. (2010). Where do winds drive the Antarctic Circumpolar Current? *Geophysical Research Letters*, *37*(12), L12605. https://doi.org/10.1029/2010GL043355

Baatsen, M. L. J., von der Heydt, A. S., Kliphuis, M., Viebahn, J., & Dijkstra, H. A. (2018). Multiple states in the late Eocene ocean circulation. *Global and Planetary Change*, *163*, 18–28. https://doi.org/10.1016/j.gloplacha.2018.02.009

Barker, P. F., Diekmann, B., & Escutia, C. (2007). Onset of Cenozoic Antarctic glaciation. *Deep-Sea Research*, *54*(21–22), 2293–2307. https://doi.org/10.1016/j.dsr2.2007.07.027

Barker, P. F., & Thomas, E. (2004). Origin, signature and palaeoclimatic influence of the Antarctic Circumpolar Current. *Earth-Science Reviews*, *66*(1–2), 143–162. https://doi.org/10.1016/j.earscirev.2003.10.003

Bijl, P. K., Bendle, J. A. P., Bohaty, S. M., Pross, J., Schouten, S., Tauxe, L., et al. (2013). Eocene cooling linked to early flow across the Tasmanian Gateway. *Proceedings of the National Academy of Sciences of the United States of America*, *110*(24), 9645–9650. https://doi.org/10.1073/pnas.1220872,110

Borrelli, C., Cramer, B. S., & Katz, M. E. (2014). Bipolar Atlantic deepwater circulation in the middle-late Eocene: Effects of Southern Ocean gateway openings. *Paleoceanography and Paleoclimatology*, *29*(4), 308–327. https://doi.org/10.1002/2012PA002444

Budyko, M. I. (1969). The effect of solar radiation variations on the climate of the Earth. *Tellus*, *21*(5), 611–619. https://doi.org/10.3402/tellusa.v21i5.10109

Cimatoribus, A. A., Drijfhout, S. S., & Dijkstra, H. A. (2014). Meridional overturning circulation: Stability and ocean feedbacks in a box model. *Climate Dynamics*, *42*(1–2), 311–328. https://doi.org/10.1007/s00382–012–1576–9

Coxall, H. K., Huck, C. E., Huber, M., Lear, C. H., Legardi-Lisarri, A., O'Regan, M., et al. (2018). Export of nutrient rich northern component water preceded early Oligocene Antarctic glaciation. *Nature Geoscience*, *11*(3), 190–196. https://doi.org/10.1038/s41,561–018–0069–9

Donohue, K. A., Tracey, K. L., Watts, D. R., Chidichimo, M. P., & Chereskin, T. K. (2016). Mean Antarctic circumpolar current transport measured in Drake Passage. *Geophysical Research Letters*, *43*(22), 11–760. https://doi.org/10.1002/2016GL070319

Durran, D. R. (1991). The third-oder Adams-Bashforth method: An attractive alternative to leapfrog time differencing. *Monthly Weather Review*, *119*(3), 702–720. https://doi.org/10.1175/1520-0493(1991)119<0702:ttoabm>2.0.co;2

Eden, C., Greatbatch, R. J., & Olbers, D. (2007). Interpreting eddy fluxes. *Journal of Physical Oceanography*, *37*(5), 1282–1296. https://doi.org/10.1175/jpo3050.1

Ferreira, D., Marshall, J., Ito, T., & McGee, D. (2018). Linking glacial-interglacial states to multiple equilibria of climate. *Geophysical Research Letters*, *45*(17), 9160–9170. https://doi.org/10.1029/2018GL077,019

Ferreira, D., Marshall, J., & Rose, B. (2011). Climate determinism revisited: Multiple equilibria in a complex climate model. *Journal of Climate*, *24*(4), 992–1012. https://doi.org/10.1175/2010jcli3580.1

Gaina, C., & Müller, D. (2007). Cenozoic tectonic and depth/age evolution of the Indonesian gateway and associated back-arc basins. *Earth-Science Reviews*, *83*(3–4), 177–203. https://doi.org/10.1016/j.earscirev.2007.04.004

Gent, P. R., & McWilliams, J. C. (1984). Balanced models in isentropic coordinates and the shallow water equations. *Tellus*, *36A*(2), 166–171. https://doi.org/10.1111/j.1600-0870.1984.tb00236.x

Gent, P. R., & McWilliams, J. C. (1990). Isopycnal mixing in ocean circulation models. *Journal of Physical Oceanography*, *20*(1), 150–155. https://doi.org/10.1175/1520-0485(1990)020<0150:imiocm>2.0.co;2

Gnanadesikan, A. (1999). A simple predictive model for the structure of the oceanic pycnocline. *Science*, *283*(5410), 2077–2079. https://doi.org/10.1126/science.283.5410.2077

Goldner, A., Herold, N., & Huber, M. (2014). Antarctic glaciation caused ocean circulation changes at the Eocene-Oligocene transition. *Nature*, *511*(7511), 574–577. https://doi.org/10.1038/nature13597

Hague, A. M., Thomas, D. J., Huber, M., Korty, R., Woodard, S. C., & Jones, L. B. (2012). Convection of North Pacific deep water during the early Cenozoic. *Geology*, *40*(6), 527–530. https://doi.org/10.1130/G32,886.1

Hallberg, R., & Gnanadesikan, A. (2001). An exploration of the role of transient eddies in determining the transport of a zonally reentrant current. *Journal of Physical Oceanography*, *31*(11), 3312–3330. https://doi.org/10.1175/1520-0485(2001)031<3312:aeotro>2.0.co;2

Hawkins, E., Smith, R. S., Allison, L. C., Gregory, J. M., Woollings, T. J., Pohlmann, H., & de Cuevas, B. (2011). Bistability of the Atlantic overturning in a global climate model and links to ocean freshwater transport. *Geophysical Research Letters*, *38*(10), L10–L605. https://doi.org/10.1029/2011GL047,208

Heiderich, J., & Todd, R. E. (2020). Along-stream evolution of Gulf Stream volume transport. *Journal of Physical Oceanography*, *50*(8), 2251–2270. https://doi.org/10.1175/JPO–D–19–0303.1

Hill, D. J., Haywood, A. M., Valdes, P. J., Francis, J. E., Lunt, D. J., Wade, B. S., & Bowman, V. C. (2013). Paleogeographic controls on the onset of the Antarctic Circumpolar Current. *Geophysical Research Letters*, *40*(19), 5199–5204. https://doi.org/10.1002/grl.50,941

Hogg, A. M. (2010). An Antarctic Circumpolar Current driven by surface buoyancy forcing. *Geophysical Research Letters*, *37*(23), L23–L601. https://doi.org/10.1029/2010GL044777

Howard, E., Hogg, A. M., Waterman, S., & Marshall, D. P. (2015). The injection of zonal momentum by buoyancy forcing in a Southern Ocean model. *Journal of Physical Oceanography*, *45*(1), 259–271. https://doi.org/10.1175/JPO–D–14–0098.1

Huber, M., & Nof, D. (2006). The ocean circulation in the southern hemisphere and its climatic impacts in the Eocene. *Palaeogeography, Palaeoclimatology, Palaeoecology*, *231*(1–2), 9–28. https://doi.org/10.1016/j.palaeo.2005.07.037

Huber, M., & Sloan, L. C. (2001). Heat transport, deep waters, and thermal gradients: Coupled simulation of an Eocene greenhouse climate. *Geophysical Research Letters*, *28*(18), 3481–3484. https://doi.org/10.1029/2001gl012943

Huck, C. E., van de Flierdt, T., Bohaty, S. M., & Hammond, S. J. (2017). Antarctic climate, Southern Ocean circulation patterns, and deep water formation during the Eocene. *Paleoceanography and Paleoclimatology*, *32*(7), 674–691. https://doi.org/10.1002/2014PA003135

Hutchinson, D. K., Coxall, H. K., O'Regan, M., Nilsson, J., Caballero, R., & de Boer, A. M. (2019). Arctic closure as a trigger for Atlantic overturning at the Eocene-Oligocene transition. *Nature Communications*, *10*(1), 3797. https://doi.org/10.1038/s41467–019–11828–z

Hutchinson, D. K., de Boer, A. M., Coxall, H. K., Caballero, R., Nilsson, J., & Baatsen, M. (2018). Climate sensitivity and meridional overturning circulation in the late Eocene using GFDL CM2.1. *Climate of the Past*, *14*(6), 789–810. https://doi.org/10.5194/cp–14–789–2018

Imawaki, S., Bower, A. S., Beal, L., & Qiu, B. (2013). *Western boundary currents, international geophysics series* (Vol. 103, pp. 305–330). Academic Press.

Jackson, L., Hughes, C. W., & Williams, R. G. (2006). Topographic control of basin and channel flows: The role of bottom pressure torques and friction. *Journal of Physical Oceanography*, *36*(9), 1786–1805. https://doi.org/10.1175/jpo2936.1

Jayne, S. R., & Marotzke, J. (2002). The oceanic eddy heat transport. *Journal of Physical Oceanography*, *32*(12), 3328–3345. https://doi.org/10.1175/1520-0485(2002)032<3328:toeht>2.0.co;2

Johnson, G. C., & Bryden, H. L. (1989). On the size of the Antarctic Circumpolar Current. *Deep-Sea Research*, *36*(1), 39–53. https://doi.org/10.1016/0198-0149(89)90017-4

Johnson, H. L., Marshall, D. P., & Sproson, D. A. J. (2007). Reconciling theories of a mechanically driven meridional overturning circulation with thermohaline forcing and multiple equilibria. *Climate Dynamics*, *29*(7–8), 821–836. https://doi.org/10.1007/s00382-007-0262-9

Jones, C. S., & Cessi, P. (2016). Interbasin transport of the meridional overturning circulation. *Journal of Physical Oceanography*, *46*(4), 1157–1169. https://doi.org/10.1175/JPO–D–15–0197.1

Jones, D. C., Ito, T., & Lovenduski, N. S. (2011). The transient response of the Southern Ocean pycnocline to changing atmospheric winds. *Geophysical Research Letters*, *38*(15), L15–L604. https://doi.org/10.1029/2011GL048145

Katz, M. E., Cramer, B. S., Toggweiler, J. R., Esmay, G., Liu, C., Miller, K. G., et al. (2011). Impact of Antarctic Circumpolar Current development on late Paleogene ocean structure. *Science*, *332*(6033), 1076–1079. https://doi.org/10.1126/science.1202122

Kennett, J. P. (1977). Cenozoic evolution of Antarctic glaciation, the circum-Antarctic ocean, and their impact on global paleoceanography. *Journal of Geophysical Research*, *82*(27), 3843–3860. https://doi.org/10.1029/jc082i027p03843

Klinger, B., & Haine, T. (2019). *Ocean circulation in three dimensions* (p. 466). Cambridge University Press.

Kuhlbrodt, T., Griesel, A., Montoya, M., Levermann, A., Hofmann, M., & Rahmstorf, S. (2007). On the driving processes of the Atlantic meridional overturning circulation. *Reviews of Geophysics*, *45*(2), RG2001. https://doi.org/10.1029/2004RG000,166

LaCasce, J. H., & Isachsen, P. E. (2010). The linear models of the ACC. *Progress in Oceanography*, *84*(3–4), 139–157. https://doi.org/10.1016/j.pocean.2009.11.002

Ladant, J. B., Donnadieu, Y., & Dumas, C. (2014). Links between CO_2, glaciation and water flow: Reconciling the Cenozoic history of the Antarctic Circumpolar Current. *Climate of the Past*, *10*(6), 1957–1966. https://doi.org/10.5194/cp–10–1957–2014

Lawrence, B. N., Bennet, V. L., Churchill, J., Juckes, M., Kershaw, P., Pascoe, S., et al. (2013). Storing and manipulating environmental big data with JASMIN. In *2013 IEEE international conference on big data* (pp. 68–75). https://doi.org/10.1109/BigData.2013.6691556

Lefebvre, V., Donnadieu, Y., Sepulchre, P., Swingedouw, D., & Zhang, Z. S. (2012). Deciphering the role of southern gateways and carbon dioxide on the onset of the Antarctic Circumpolar Current. *Paleoceanography*, *27*(4), PA4201. https://doi.org/10.1029/2012PA002,345

Livermore, R., Nankivell, A., Eagles, G., & Morris, P. (2005). Paleogene opening of Drake Passage. *Earth and Planetary Science Letters*, *236*(1–2), 459–470. https://doi.org/10.1016/j.epsl.2005.03.027

Mak, J., Maddison, J. R., Marshall, D. P., & Munday, D. R. (2018). Implementation of a geometrically informed and energetically constrained mesoscale eddy parameterization in an ocean circulation model. *Journal of Physical Oceanography*, *48*(10), 2363–2382. https://doi.org/10.1175/JPO–D–18.0017.1

Marotzke, J., & Willebrand, J. (1991). Multiple equilibria of the global thermohaline circulation. *Journal of Physical Oceanography*, *21*(9), 1372–1385. https://doi.org/10.1175/1520-0485(1991)021<1372:meotgt>2.0.co;2

Marshall, D. (1995). Topographic steering of the Antarctic Circumpolar Current. *Journal of Physical Oceanography*, *25*(7), 1636–1650. https://doi.org/10.1175/1520-0485(1995)025<1636:tsotac>2.0.co;2

Marshall, D. P. (2011). Rossby wormholes. *Journal of Marine Research*, *69*(2), 309–330. https://doi.org/10.1357/002224011798765,213

Marshall, D. P., Maddison, J. R., & Berloff, P. S. (2012). A framework for parameterizing eddy potential vorticity fluxes. *Journal of Physical Oceanography*, *42*(4), 539–557. https://doi.org/10.1175/JPO–D–11–048.1

Marshall, D. P., Munday, D. R., Allison, L. C., Hay, R. J., & Johnson, H. L. (2016). Gill's model of the Antarctic Circumpolar Current, revisited: The role of latitudinal variations in wind stress. *Ocean Modelling*, *97*, 37–51. https://doi.org/10.1016/j.ocemod.2015.11.010

Marshall, D. P., & Pillar, H. R. (2011). Momentum balance of the wind-driven and meridional overturning circulation. *Journal of Physical Oceanography*, *41*(5), 960–978. https://doi.org/10.1175/2011JPO4528.1

Marshall, D. P., & Zanna, L. (2014). A conceptual model of ocean heat uptake under climate change. *Journal of Climate*, *27*(22), 8444–8465. https://doi.org/10.1175/JCLI–D–13–00,344.1

Marshall, J., & Radko, T. (2003). Residual-mean solutions for the Antarctic Circumpolar Current and its associated overturning circulation. *Journal of Physical Oceanography*, *33*(11), 2341–2354. https://doi.org/10.1175/1520-0485(2003)033<2341:rsftac>2.0.co;2

Marshall, J., & Speer, K. (2012). Closure of the meridional overturning circulation through Southern Ocean upwelling. *Nature Geoscience*, *5*(3), 171–180. https://doi.org/10.1038/ngeo1391

Mazloff, M. R., Heimbach, P., & Wunsch, C. (2010). An eddy-permitting Southern Ocean state estimate. *Journal of Physical Oceanography*, *40*(5), 880–899. https://doi.org/10.1175/2009JPO4236.1

McKinley, C. C., Thomas, D. J., LeVay, L. J., & Rolewicz, Z. (2019). Nd isotopic structure of the Pacific Ocean 40-10 Ma and evidence for the reorganization of deep North Pacific Ocean circulation between 36 and 35 Ma. *Earth and Planetary Science Letters*, *521*, 139–149. https://doi.org/10.1016/j.epsl.2019.06.009

Meinen, C. S., Baringer, M. O., & Garcia, R. F. (2010). Florida Current transport variability: An analysis of annual and longer-period signals. *Deep-Sea Research*, *57*(7), 835–846. https://doi.org/10.1016/j.dsr.2010.04.001

Meredith, M. P., Woodworth, P. L., Chereskin, T. K., Marshall, D. P., Allison, L. C., Bigg, G. R., et al. (2011). Sustained monitoring of the Southern Ocean at Drake Passage: Past achievements and future priorities. *Reviews of Geophysics*, *49*(4), RG4005. https://doi.org/10.1029/2010RG000348

Munday, D. (2022). davemunday/reducedgravity: v1.0.1 [Software]. *Zenodo*. https://doi.org/10.5281/zenodo.7078679

Munday, D. R., Johnson, H. L., & Marshall, D. P. (2013). Eddy saturation of equilibrated circumpolar currents. *Journal of Physical Oceanography*, *43*(3), 507–532. https://doi.org/10.1175/JPO–D–12–095.1

Munday, D. R., Johnson, H. L., & Marshall, D. P. (2015). The role of ocean gateways in the dynamics and sensitivity to wind stress of the early Antarctic Circumpolar Current. *Paleoceanography*, *30*(3), 284–302. https://doi.org/10.1002/2014PA002675

Munday, D. R., Sauermilch, I., Whittaker, J., & Klocker, A. (2022). Opening of Tasman seaway and the Antarctic Circumpolar Current [Dataset]. *Open Science Framework*. https://doi.org/10.17605/OSF.IO/PQYMU

Munk, W. H. (1950). On the wind-driven ocean circulation. *Journal of Meteorology*, *7*(2), 79–93. https://doi.org/10.1175/1520-0469(1950)007<0080:otwdoc>2.0.co;2

Munk, W. H., & Palmén, E. (1951). Note on the dynamics of the Antarctic Circumpolar Current. *Tellus*, *3*(1), 53–55. https://doi.org/10.3402/tellusa.v3i1.8609

Nof, D. (2000a). Why much of the Atlantic circulation enters the Caribbean Sea and very little of the Pacific circulation enters the Sea of Japan. *Progress in Oceanography*, *45*(1), 39–67. https://doi.org/10.1016/s0079-6611(99)00050-6

Nof, D. (2000b). Does the wind control the import and export of the South Atlantic? *Journal of Physical Oceanography*, *30*(11), 2650–2666. https://doi.org/10.1175/1520-0485(2000)030<2650:dtwcti>2.0.co;2

Nof, D. (2002). Is there a meridional overturning cell in the Pacific and Indian oceans? *Journal of Physical Oceanography*, *32*(6), 1947–1959. https://doi.org/10.1175/1520-0485(2002)032<1947:itamoc>2.0.co;2

Nof, D. (2003). The Southern Ocean's grip on the northward meridional flow. *Progress in Oceanography*, *56*(2), 223–247. https://doi.org/10.1016/s0079-6611(03)00005-3

Nof, D., & Van Gorder, S. (2003). Did an open Panama Isthmus correspond to an invasion of Pacific water into the Atlantic? *Journal of Physical Oceanography*, *33*(7), 1324–1336. https://doi.org/10.1175/1520-0485(2003)033<1324:daopic>2.0.co;2

Pillar, H. R. (2013). Sensitivity of the Atlantic meridional overturning circulation to surface forcing. Ph.D. thesis. University of Oxford.

Rose, B. E. J. (2015). Stable "Waterbelt" climates controlled by tropical ocean heat transport: A nonlinear coupled climate mechanism of relevance to Snowball Earth. *Journal of Geophysical Research*, *120*(4), 1404–1423. https://doi.org/10.1002/2014DJ022659

Rose, B. E. J., Ferreira, D., & Marshall, J. (2013). The role of oceans and sea ice in abrupt transitions between multiple climate states. *Journal of Climate*, *26*(9), 2862–2879. https://doi.org/10.1175/JCLI–D–12–00,175.1

Royer, J. Y., & Rollet, N. (1997). Plate-tectonic setting of the Tasmanian region. *Australian Journal of Earth Sciences*, *44*(5), 543–560. https://doi.org/10.1080/08120099708728336

Sauermilch, I., Whittaker, J. M., Bijl, P. K., Totterdell, J. M., & Jokat, W. (2019). Tectonic, oceanographic, and climatic controls on the Cretaceous-Cenozoic sedimentary record of the Australian-Antarctic basin. *Journal of Geophysical Research*, *124*(8), 7699–7724. https://doi.org/10.1029/2018JB016683

Sauermilch, I., Whittaker, J. M., Klocker, A., Munday, D. R., Hochmuth, K., LaCasce, J. H., & Bijl, P. K. (2021). Gateway-driven weakening of ocean gyres leads to Southern Ocean cooling. *Nature Communications*, *12*(1), 6465. https://doi.org/10.1038/s41467–021–26,658–1

Scher, H. D., & Martin, E. E. (2006). Timing and climatic consequences of the opening of Drake Passage. *Science*, *312*(5772), 428–430. https://doi.org/10.1126/science.1120,044

Scher, H. D., Whittaker, J. M., Williams, S. E., Latimer, J. C., Kordesch, W. E., & Delaney, M. L. (2015). Onset of Antarctic Circumpolar Current 30 million years ago as Tasmanian Gateway aligned with westerlies. *Nature*, *523*(7562), 580–583. https://doi.org/10.1038/nature14598

Sellers, W. D. (1969). A global climatic model based on the energy balance of the Earth-atmosphere system. *Journal of Applied Meteorology*, *8*(3), 392–400. https://doi.org/10.1175/1520-0450(1969)008<0392:agcmbo>2.0.co;2

Shakespeare, C. J., & Hogg, A. M. (2012). An analytical model of the response of the meridional overturning circulation to changes in wind and buoyancy forcing. *Journal of Physical Oceanography*, *42*(8), 1270–1287. https://doi.org/10.1175/JPO–D–11–0198.1

Sijp, W. P., England, M. H., & Huber, M. (2011). Effect of the deepening of the Tasman Gateway on the global ocean. *Paleoceanography*, *26*(4), PA4207. https://doi.org/10.1029/2011PA002143

Sijp, W. P., von der Heydt, A. S., Dijkstra, H. A., Flögel, S., Douglas, P. M. J., & Bijl, P. K. (2014). The role of ocean gateways on cooling climate on long time scales. *Global and Planetary Change*, *119*, 1–22. https://doi.org/10.1016/j.gloplacha.2014.04.004

Sloyan, B. M., Ridgway, K. R., & Cowley, R. (2016). The East Australian Current and property transport at 27 S from 2012 to 2013. *Journal of Physical Oceanography*, *46*(3), 993–1008. https://doi.org/10.1175/JPO–D–15–0052.1

Speich, S., Blanke, B., & Cai, W. (2007). Atlantic meridional overturning circulation and the southern hemisphere supergyre. *Geophysical Research Letters*, *34*(23), L23–L614. https://doi.org/10.1029/2007GL031,583

Stewart, A. L., & Hogg, A. M. (2017). Reshaping the Antarctic Circumpolar Current via Antarctic bottom water export. *Journal of Physical Oceanography*, *47*(10), 2577–2601. https://doi.org/10.1175/JPO–D–17–0007.1

Stickley, C. E., Brinkhuis, H., Schellenberg, S. A., Sluijs, A., Röhl, U., Fuller, M., et al. (2004). Timing and nature of the deepening of the Tasmanian Gateway. *Paleoceanography*, *19*(4), PA4027. https://doi.org/10.1029/2004PA001,022

Stommel, H. (1948). The westward intensification of wind-driven ocean currents. *Transactions - American Geophysical Union*, *29*, 202–206.

Stommel, H. (1961). Thermohaline circulation with two stable regimes of flow. *Tellus*, *13*(2), 224–230. https://doi.org/10.3402/tellusb.v13i2.12985

Straume, E. O., Nummelin, A., Gaina, C., & Nisancioglu, K. H. (2022). Climate transition at the Eocene-Oligocene influenced by bathymetric changes to the Atlantic-Arctic oceanic gateways. *Proceedings of the National Academy of Sciences of the United States of America*, *119*(17), e2115346119. https://doi.org/10.1073/pnas.2115346,119

Tansley, C. E., & Marshall, D. P. (2001). On the dynamics of wind-driven circumpolar currents. *Journal of Physical Oceanography*, *31*(11), 3258–3273. https://doi.org/10.1175/1520-0485(2001)031<3258:otdowd>2.0.co;2

Thomas, D. J. (2004). Evience for deep-water production in the North Pacific Ocean during the early Cenozoic warm interval. *Nature*, *430*(6995), 65–68. https://doi.org/10.1038/nature02639

Thomas, D. J., Korty, R., Huber, M., Schubert, J. A., & Haines, B. (2014). Nd isotopic structure of the Pacific Ocean 70-30 Ma and numerical evidence for vigorous ocean circulation and ocean heat transport in a greenhouse world. *Paleoceanography*, *29*(5), 454–469. https://doi.org/10.1002/2013PA002535

Toumoulin, A., Donnadieu, Y., Ladant, J. B., Batenburg, S. J., Poblete, F., & Dupont-Nivet, G. (2020). Quantifying the effect of the Drake Passage opening on the Eocene ocean. *Paleoceanography and Paleoclimatology*, *35*(8), e2020PA003889. https://doi.org/10.1029/2020PA003889

Vahlenkamp, M., Niezgodzki, I., De Vleeschouwer, D., Lohmann, G., Bickert, T., & Pälike, H. (2018). Ocean and climate response to North Atlantic seaway changes at the onset of long-term Eocene cooling. *Earth and Planetary Science Letters*, *498*, 185–195. https://doi.org/10.1016/j.epsl.2018.06.031

Vallis, G. (2017). *Atmospheric and oceanic fluid dynamics* (p. 946). Cambridge University Press. https://doi.org/10.1017/9781107588417

van de Lagemaat, S. H. A., Swart, M. L. A., Vaes, B., Kosters, M. E., Boschman, L. M., Burton-Johnson, A., et al. (2021). Subduction initiation in the Scotia Sea region and opening of the Drake Passage: When and why? *Earth-Science Reviews*, *215*, 103–551. https://doi.org/10.1016/j.earscirev.2021.103,551

Via, R. K., & Thomas, D. J. (2006). Evolution of Atlantic thermohaline circulation: Early Oligocene onset of deep-water production in the North Atlantic. *Geology*, *34*(6), 441–444. https://doi.org/10.1130/G22,545.1

Viebahn, J., & Eden, C. (2010). Towards the impact of eddies on the response of the Southern Ocean to climate change. *Ocean Modelling*, *34*(3–4), 150–165. https://doi.org/10.1016/j.ocemod.2010.05.005

Visbeck, M., Marshall, J., Haine, T., & Spall, M. (1997). Specification of eddy transfer coefficients in coarse-resolution ocean circulation models. *Journal of Physical Oceanography*, *27*(3), 381–402. https://doi.org/10.1175/1520-0485(1997)027<0381:soetci>2.0.co;2

von der Heydt, A., & Dijkstra, H. A. (2008). The effect of gateways on ocean circulation patterns in the Cenozoic. *Global and Planetary Change*, *62*(1–2), 132–146. https://doi.org/10.1016/j.gloplacha.2007.11.006

Ward, M. L., & Hogg, A. M. (2011). Establishment of momentum balance by form stress in a wind-driven channel. *Ocean Modelling*, *40*(2), 133–146. https://doi.org/10.1016/j.ocemod.2011.08.004

Webb, D. J. (1993). A simple model of the effect of the Kerguelen Plateau on the strength of the Antarctic Circumpolar Current. *Geophysical & Astrophysical Fluid Dynamics*, *70*(1–4), 57–84. https://doi.org/10.1080/03091929308203,587

Wei, W., & Wise, S. W. (1992). Eocene-Oligocene calcareous nannofossil magnetobiochrononology of the Southern Ocean. *Newsletters on Stratigraphy*, *26*(2–3), 119–132. https://doi.org/10.1127/nos/26/1992/119

Westerhold, T., Marwan, N., Drury, A. J., Liebrand, D., Agnini, C., Anagnostou, E., et al. (2020). An astronomically dated record of Earth's climate and its predictability over the last 66 million years. *Science*, *369*(6509), 1383–1387. https://doi.org/10.1126/science.aba6853

Xing, Q., Klocker, A., Munday, D., & Whittaker, J. (2023). Deep convection as the key to the transition from Eocene to modern Antarctic Circumpolar Current. *Geophysical Research Letters*, *50*(24), e2023GL104847. https://doi.org/10.1029/2023GL104,847

Xing, Q., Munday, D., Klocker, A., Sauermilch, I., & Whittaker, J. (2022). The sensitivity of the Eocene-Oligocene Southern Ocean to the strength and position of wind stress. *Climate of the Past*, *18*(12), 2669–2693. https://doi.org/10.5194/cp–18–2669–2022

Youngs, M. K., Flierl, G. R., & Ferrari, R. (2019). Role of residual overturning for the sensitivity of Southern Ocean isopycnal slopes to changes in wind forcing. *Journal of Physical Oceanography*, *49*(11), 2867–2881. https://doi.org/10.1175/JPO–D–19–0072.1

Zhang, Y., de Boer, A. M., Lunt, D. J., Hutchinson, D. K., Ross, P., van de Flierdt, T., et al. (2022). Early Eocene ocean meridional overturning circulation: The roles of atmospheric forcing and strait geometry. *Paleoceanography and Paleoclimatology*, *37*(3), e2021PA004329. https://doi.org/10.1029/2021PA004,329